Dist: A

AD-A284 780

...ON PAGE

Form Approved
OMB No. 0704-0188

1. AGENCY USE ONLY (Leave blank)	2. REPORT DATE	3. REPORT TYPE AND DATES COVERED
	August 31, 1994	Final 01 July 91 - 30 June 94

4. TITLE AND SUBTITLE

(U) Combustion Instability Phenomena of Importance to Liquid Propellant Engines

5. FUNDING NUMBERS

PE - 61102F
PR - 2308
SA - A1
G - AFOSR-91-0336

6. AUTHOR(S)

R.J. Santoro and W.E. Anderson

7. PERFORMING ORGANIZATION NAME(S) AND ADDRESS(ES)

The Pennsylvania State University
240 Research Building East, Bigler Road
University Park, PA 16802-2320

8. PERFORMING ORGANIZATION REPORT NUMBER

AFOSR-TR- 94 0578

9. SPONSORING / MONITORING AGENCY NAME(S) AND ADDRESS(ES)

AFOSR/NA
110 Duncan Avenue, Suite B115
Bolling AFB, DC 20332-0001

10. SPONSORING / MONITORING AGENCY REPORT NUMBER

DTIC ELECTE SEP 23 1994 F

11. SUPPLEMENTARY NOTES

12a. DISTRIBUTION / AVAILABILITY STATEMENT

Approved for public release; distribution is unlimited.

94 9 22 005 A

12b. DISTRIBUTION CODE

13. ABSTRACT *(Maximum 200 words)*

A systematic study of the atomization of impinging liquid jets was performed. Effects of jet flow condition, orifice diameter, impingement angle, pre-impingment length, fabrication procedure, and jet velocity at steady and oscillating, and atmospheric- and high-pressure ambient conditions were investigated. Measurements of sheet breakup length, drop size and velocity distribution, and the length between sheet structures and detached ligaments were made. Results of the experiments were compared to theoretical predictions. It appears that primary breakup of the sheets formed by turbulent impinging jets is controlled by pressure and momentum fluctuations in the liquid that are accentuated near the impingement point and that have their origin in the jet prior to impingement. Based on these results, approaches to modeling impinging jet atomization should focus on pre-impingement jet conditions and the physics near the jet impingement point. Experimental results were also studied in the context of an empirical correlation used in industry for the prediction of combustion stability. The frequency with which the periodic disturbances that control primary breakup are formed has a marked similarity to the combustion instability frequency predicted by the stability correlation. Furthermore, an increase in predicted stability coincides with an increase in measured mean drop size and an increase in the polydispersity of the drop size distribution.

DTIC QUALITY INSPECTED 8

94-30456

14. SUBJECT TERMS	15. NUMBER OF PAGES
Impinging jet injectors; combustion instability; atomization	78
	16. PRICE CODE

17. SECURITY CLASSIFICATION OF REPORT	18. SECURITY CLASSIFICATION OF THIS PAGE	19. SECURITY CLASSIFICATION OF ABSTRACT	20. LIMITATION OF ABSTRACT
UNCLASSIFIED	UNCLASSIFIED	UNCLASSIFIED	UL

GENERAL INSTRUCTIONS FOR COMPLETING SF 298

The Report Documentation Page (RDP) is used in announcing and cataloging reports. It is important that this information be consistent with the rest of the report, particularly the cover and title page. Instructions for filling in each block of the form follow. It is important to ***stay within the lines*** to meet ***optical scanning requirements***.

Block 1. Agency Use Only *(Leave blank)*.

Block 2. Report Date. Full publication date including day, month, and year, if available (e.g. 1 Jan 88). Must cite at least the year.

Block 3. Type of Report and Dates Covered. State whether report is interim, final, etc. If applicable, enter inclusive report dates (e.g. 10 Jun 87 - 30 Jun 88).

Block 4. Title and Subtitle. A title is taken from the part of the report that provides the most meaningful and complete information. When a report is prepared in more than one volume, repeat the primary title, add volume number, and include subtitle for the specific volume. On classified documents enter the title classification in parentheses.

Block 5. Funding Numbers. To include contract and grant numbers; may include program element number(s), project number(s), task number(s), and work unit number(s). Use the following labels:

C	- Contract	**PR**	- Project
G	- Grant	**TA**	- Task
PE	- Program Element	**WU**	- Work Unit Accession No.

Block 6. Author(s). Name(s) of person(s) responsible for writing the report, performing the research, or credited with the content of the report. If editor or compiler, this should follow the name(s).

Block 7. Performing Organization Name(s) and Address(es). Self-explanatory.

Block 8. Performing Organization Report Number. Enter the unique alphanumeric report number(s) assigned by the organization performing the report.

Block 9. Sponsoring/Monitoring Agency Name(s) and Address(es). Self-explanatory.

Block 10. Sponsoring/Monitoring Agency Report Number. *(If known)*

Block 11. Supplementary Notes. Enter information not included elsewhere such as: Prepared in cooperation with...; Trans. of...; To be published in.... When a report is revised, include a statement whether the new report supersedes or supplements the older report.

Block 12a. Distribution/Availability Statement. Denotes public availability or limitations. Cite any availability to the public. Enter additional limitations or special markings in all capitals (e.g. NOFORN, REL, !TAR).

- **DOD** - See DoDD 5230.24, "Distribution Statements on Technical Documents."
- **DOE** - See authorities.
- **NASA** - See Handbook NHB 2200.2.
- **NTIS** - Leave blank.

Block 12b. Distribution Code.

- **DOD** - Leave blank.
- **DOE** - Enter DOE distribution categories from the Standard Distribution for Unclassified Scientific and Technical Reports.
- **NASA** - Leave blank.
- **NTIS** - Leave blank.

Block 13. Abstract. Include a brief *(Maximum 200 words)* factual summary of the most significant information contained in the report.

Block 14. Subject Terms. Keywords or phrases identifying major subjects in the report.

Block 15. Number of Pages. Enter the total number of pages.

Block 16. Price Code. Enter appropriate price code *(NTIS only)*.

Blocks 17. - 19. Security Classifications. Self-explanatory. Enter U.S. Security Classification in accordance with U.S. Security Regulations (i.e., UNCLASSIFIED). If form contains classified information, stamp classification on the top and bottom of the page.

Block 20. Limitation of Abstract. This block must be completed to assign a limitation to the abstract. Enter either UL (unlimited) or SAR (same as report). An entry in this block is necessary if the abstract is to be limited. If blank, the abstract is assumed to be unlimited.

Final Report
on
Combustion Instability Phenomena of Importance to Liquid Propellant Engines

Prepared by:

Robert J. Santoro and William E. Anderson
Department of Mechanical Engineering
and
Propulsion Engineering Research Center
The Pennsylvania State University
University Park, PA 16802 - 2320

Submitted to:

Air Force Office of Scientific Research
Bolling Air Force Base
Washington, D.C.

July 1994

TABLE OF CONTENTS

1.0 RESEARCH OBJECTIVE

Impinging jet injectors are a common type of injector used in liquid rocket engines and are typically used in engines where both propellants are injected as a liquid, e.g., engines using LOX/hydrocarbon and storable propellant combinations. Because they are much simpler to fabricate than coaxial injectors, they are also an attractive candidate for use in LOX/hydrogen engines. There are also current interests in engines where both propellants are injected as gas and where three propellants are used; here, the impinging jet injector system would also be favored over coaxial jets due to superior mixing characteristics and potentially simpler manifolding arrangement.

The current state of impinging jet injector design analysis, however, significantly lags behind that for coaxial elements. A substantial problem exists with the current design analysis methodology for impinging jet injectors in that to increase the margin from unstable combustor operation, the combustor designer is faced with decrementing performance and thermal compatibility characteristics. Also, empirically-based analysis techniques are used which depend, of course, on existing engine data. Due to the empirical nature of stability analysis, and the very high costs of engine development, innovative designs that take advantage of current technology are not being used; instead, current engines are essentially being built with the same injector designs that were developed in the 1960's.

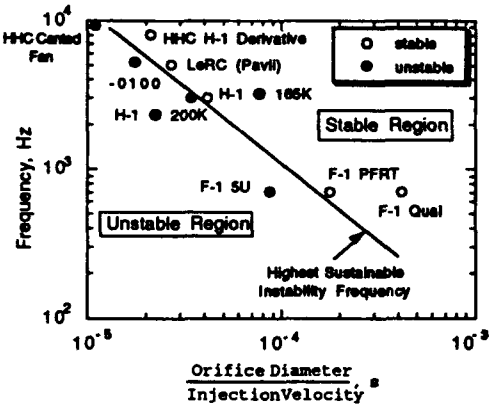

Fig 1. Hewitt stability correlation for determining the highest possible combustion instability frequency in rocket engines using impinging jet injectors as a function of injector stability parameter. Correlation effectiveness is illustrated by a few examples of LOX/hydrocarbon engines.

The research program at the Propulsion Engineering Research Center at Penn State has been focused on providing the requisite fundamental understanding for the development of an advanced, *a priori* combustion stability design analysis capability. This can only be achieved when the fundamental mechanisms of combustion stability in rocket engines using impinging jet injectors are understood. A key element of the program's approach was the use of a proven empirical stability correlation, previously a proprietary design tool at Aerojet shown in Fig. 1, that relates the highest possible frequency of combustion instability that can be driven by an injector with given geometric and operational parameters, i.e., injector diameter and injection velocity. A review and characteristic time analysis of potential combustion instability mechanisms that explain the correlation has been performed,[1] resulting in the identification of

the processes of primary and secondary atomization, inter-propellant mixing, and vaporization as likely important controlling steps. Identification of these processes was used to define the dependent test variables to be measured: length of the intact liquid sheet, ligament shedding frequency, drop size and velocity distribution, and heat release rate. The empirical correlation was used to define independent test parameters: orifice diameter, injection velocity, and imposed frequency of oscillation.

The results of the review also indicated that a clear understanding of primary atomization is of particular importance. Studies of primary atomization have shown that it occurs on a temporal scale that is similar in magnitude to combustion instability, and that the temporal dependency on orifice diameter and injection velocity is similar to the dependency indicated by the combustion stability correlation used in the present study. Furthermore, inter-propellant mixing and drop vaporization and burning are controlled by the distribution of drop size and velocity which is determined by primary atomization. Thus, the major effort has been to characterize the injector's geometric and flow effects on primary atomization and to develop a reliable and accurate atomization model for impinging jets.

In summary, the overall objective of this study was to determine the physical mechanisms that are responsible for the combustion stability characteristics of rocket engines that use impinging jet injectors, using a proven empirical correlation to link the fundamental study to practical rocket combustors. Additionally, the most complete and systematic study of the atomization of impinging liquid jets to date has been completed under this contract. Effects of jet flow condition, orifice diameter, impingement angle, pre-impingment length, fabrication procedure, and jet velocity at steady and oscillating, and atmospheric- and high-pressure conditions have been investigated. From these cold-flow tests, three important observations related to the basis of the stability correlation have been made: (1) as the stability parameter is increased, leading to more stable operation, the spray drop size distribution becomes more polydisperse; (2) as the stability parameter is increased, the mean drop size is increased; and (3) the frequency with which ligaments are formed and with which waves of drops enter the combustion zone has a functional dependence on the stability parameter similar to that of the maximum predicted instability frequency as shown in Fig. 1.

The results of this study have contributed to a fundamental understanding of the atomization processes and the operative instability mechanisms associated with impinging jet injectors. These results must still be verified under combusting-flow conditions. Also, more work needs to be done to relate the observed phenomenology to specific physical processes to enable development of *a priori* design analysis methodologies and implementation of engineering control strategies for future design of stable, high-performing, and thermally compatible rocket combustors.

2.0 RESULTS

The subject study was concentrated on defining the operative mechanisms of combustion instability in rocket engines that use impinging jet injectors. General information regarding the combustion process in rocket engine combustors of all types is also an important byproduct of this research. A review conducted earlier[1] identified the combustion processes of primary atomization, secondary atomization, inter-propellant mixing, and drop heating, vaporization, and burning as potential key mechanisms of combustion instability. The effort involved cold-flow studies of atomization under both steady and forced oscillatory ambient conditions. There has also been a parallel effort in developing an accurate atomization model. More details of the work can be found in References 1 - 3, and in Appendix 1. Future studies under high-pressure, combusting, and oscillatory conditions must still be undertaken to verify the cold-flow results and to measure the combustion response of impinging liquid jet spray combustion in terms of the phase relationship between the oscillating pressure field and combustion.

The development of a clear and detailed understanding of atomization was emphasized in the study for two reasons: (1) atomization provides the initial conditions for subsequent combustion processes by its determinant effect on drop size and velocity; and (2) the periodic nature of primary atomization (ligament shedding) has pronounced similarities to combustion oscillations in rocket engines in terms of both frequency range and the frequency dependency on injector operational and geometric parameters.

The three classical cases of fully-developed laminar jet flow, fully-developed turbulent jet flow, and "plug" jet flow were studied. These cases were chosen because of their well-characterized velocity and turbulence intensity profiles. Absolute plug flow conditions were not obtained, but were approached by using orifices with short length-to-diameter ratios (L/d_o~5). Length-to-diameter ratios in impinging jet orifices used in rocket engines are typically about three to five. In addition to changing flow condition and L/d_o, other test parameters (see Table 1) included impingement angle, 2θ, orifice diameter, and free jet length prior to impingement.

It was obvious that the flow condition of the jet before impingement, i.e., whether it was laminar or turbulent, had the major effect on atomization. To illustrate the importance of the initial conditions of the liquid jet, consider the instantaneous images of the sheets formed by laminar and turbulent impinging jets shown in Fig. 2. These images were taken under quiescent conditions and at atmospheric pressure. Although the jet Reynolds numbers for both the laminar and turbulent cases are similar, the resultant sheets have very different and distinct characteristics. In the laminar case, Fig. 2a, small ripples on the surface of the sheet are seen near the impingement point, and after some distance the sheet suddenly disintegrates into drops. In

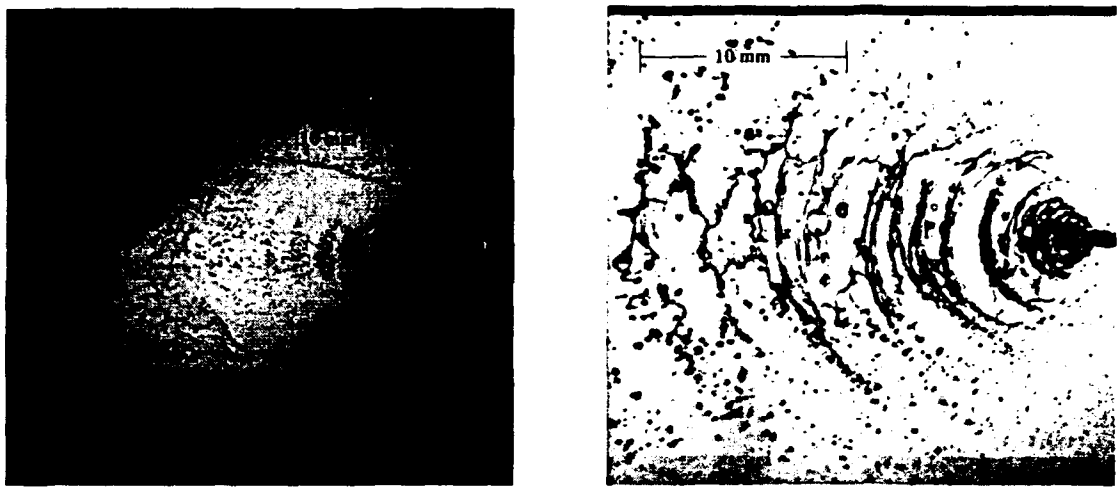

(a) (b)

Fig. 2. Instantaneous images of sprays formed by two impinging water jets. (a) Resultant sheet formed by two laminar impinging jets emanating from 0.51 mm inner diameter, L/d_0=375 precision bore glass tubes. The jet velocity was 13.1 m/s and the full impingement angle, 2θ, was 60^0. (b) Resultant sheet formed by two turbulent impinging jets emanating from 0.64 mm inner diameter, L/d_0=80 precision bore glass tubes. The jet velocity was 12.2 m/s and the full impingement angle, 2θ, was 60^0.

many of the images of laminar impinging jets, incipient breakup occurred at mid-span of the sheet. Drops are also seen shedding steadily off the edge of the sheet. In the turbulent case, Fig. 2b, the waves that appear at impact are larger than in the laminar case. Downstream, the sheet disintegrates into ligaments, with incipient breakup consistently occurring at the edges where the sheet is thinnest. Periodicity is indicated by waves on the liquid sheet and by the spacing between the detached ligaments. Examination of the detached liquid structures reveals irregular liquid shapes that contract into roughly cylindrical ligaments. The cylindrical ligaments appear to contract further into irregularly-shaped drops that will eventually take a nearly spherical shape. The ligament-to-droplet formation process at atmospheric pressure is most likely controlled by surface tension-driven instabilities, and by a combined surface tension - aerodynamic effect at higher ambient pressures.

The turbulent sheet is not as symmetric as the laminar sheet, and, by comparing upstream and downstream points near the edge of the turbulent sheet there appears to be relatively large-scale displacement of the sheet in the image plane, indicating jet unsteadiness on the large scale. Examination of opposite edges at the same downstream location leads to the same conclusion regarding asymmetry and large-scale jet unsteadiness. This phenomena is in all probability three-dimensional.

From the results presented in Fig. 2, it is clear that the phenomena controlling atomization for impinging jet injectors is complicated and requires both theoretical and experimental study. Thus, emphasis has been given to comparing the non-vaporizing

atmospheric impinging jet studies with theoretical models as well as extending the experimental work to higher ambient pressures and forced oscillatory conditions.

Table 1. Atomization Characterization Test Conditions

	Injector Type		
Test Parameter	Glass Tubes	Twist-Drilled	EDM
Orifice Diameter, mm	0.51, 0.64, 1.02, 1.45	1.02	0.51
Impingment Angle, degrees	40, 60, 80, 100, 180	60	60
Length-to-Diameter Ratio	5, 35, 50, 80, 375	10	5
Pre-impingement Length, mm	2.5, 25, 35	14	2.5
Laminar Flow Conditions:	$2800<Re_j<10000$	N/A	N/A
	$200<We_j<2300$		
Turbulent Flow Conditions:	$4000<Re_j<30000$	$3000<Re_j<20000$	$4000<Re_j<30000$
	$300<We_j<7000$	$150<We_j<4000$	$300<We_j<7000$
Ambient Pressure	1	1, 6, 9	1, 5, 10
Acoustic Frequency, Hz	N/A	670,1360,2020	N/A
Acoustic Pressure, kPa (psi) (peak - peak amplitude)	N/A	1.4 - 6.2 (0.2 - 0.9)	N/A

2.1 Modeling Results

The significant task of developing a mechanistic model of primary atomization was undertaken as part of this contract. A mechanistic model that can accurately predict the effects of injector design and operation on breakup length, atomization frequency, and drop size and velocity distributions is critically needed by combustor designers. Two types of models have been studied for their usefulness for predicting impinging jet atomization: (1) a linear stability - based model that was used to provide predictions of breakup length, fastest growing wavelength, and mean drop size predictions; and (2) a finite difference model that was used to study the effects of jet disturbances and jet - jet interactions on incipient wave formation on the liquid sheet.

2.1.1 Linear Stability Model

The atomization model that has been used to date by most workers in this area[4,5,6] is based on a linear stability analysis of aerodynamically-induced wave growth on the surface of a thinning, viscous liquid sheet. This model was used to predict breakup length, the periodic structure of breakup, and drop size. Details of our implementation of the model as well as a more detailed comparison with the present experimental results can be found in References 2 and 3 and Appendix 1.

In brief, the linear stability model is based on the growth of infinitesimal disturbances due to aerodynamic stresses on the liquid sheet surface to describe the disintegration of liquid sheets. The disturbance on the sheet surface, η, is given by

$$\frac{\eta}{\eta_o} = e^{\beta_i t} \qquad (1)$$

where η_o is the initial displacement amplitude, β_i is the growth rate and t is time.

Typically the growth rate, β_i ,is calculated for a spectrum of wavenumbers, k. The disturbance wavenumber corresponding to the maximum growth rate, $\beta_{i,m}$, controls the breakup process. Both sinuous (antisymmetric) and dilatational (symmetric) waves can grow; however, previous research indicates that sinuous waves grow faster than dilatational waves,[6] hence only the behavior of sinuous disturbances were considered. The theory does not predict a critical disturbance amplitude for sheet disintegration, and consequently, an empirical relation of the following form is typically used:[2]

$$\int_0^{t_b} \beta_{i,m} dt = \int_0^{x_b} \frac{\beta_{i,m}}{U_s} dx = 12 \qquad (2)$$

where t_b is the sheet breakup time, x_b is the breakup length, and U_s is the sheet velocity. The fastest growing wave and its growth rate are found from the general dispersion equation:

$$\beta^2_{i,nd} + \frac{(kh)^2}{Re_s}\beta_{i,nd} + 2s(kh)^2\left(\frac{1}{sWe_s} - \frac{1}{kh}\right) = 0 \qquad (3)$$

where;

$$\beta_{i,nd} = \frac{\beta_i h}{U_s}, \qquad Re_s = \frac{\rho_l U_s h}{\mu_l}, \qquad We_s = \frac{\rho_l U_s^2 h}{\sigma}$$

where h is the sheet thickness and s is the ratio of the gas density to the liquid density. The first term in Equation (3) is associated with momentum in the displacement direction, the second term rises from viscous forces while the two parts of the third term account for surface tension forces and aerodynamic forces, respectively. Drop size can also be calculated by assuming the sinuous waves that are formed on the sheet break at their crests and troughs and subsequently contract into cylindrical ligaments with diameter d_L. Drops are formed when the cylindrical ligaments undergo the well-known process of capillary instability and pull themselves into spheres (drops) with a diameter, d_D, which, under the conditions of the present study, can be expressed by

$$d_D \approx 1.89 d_L \qquad (4)$$

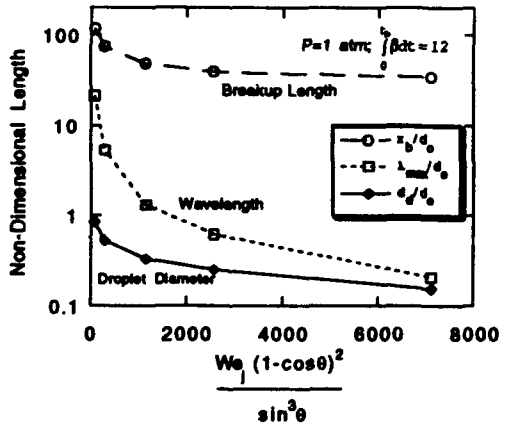

Fig. 3. Non-dimensional lengths as a function of geometrically scaled jet Weber number as predicted by aerodynamic instability model. Lengths normalized by orifice diameter.

In the course of analyzing results from the aerodynamic stability model, a non-dimensional scaling parameter based on the jet Weber number, $We_j = \rho_j v_j^2 d_o/\sigma$, and the half-impingement angle, θ, was identified: $We_j(1-\cos\theta)^2/\sin^3\theta$. Use of this parameter collapses the theoretical dependence of breakup length, fastest-growing wavelength, and drop size on orifice diameter, impingement angle, and velocity into a single curve dependent on the scaling parameter. Results from the model are shown in Fig. 3, where non-dimensional lengths, normalized by the orifice diameter, d_o, are plotted against the geometrically scaled jet Weber number.

2.1.2 Finite Difference Model

The formation of large impact waves on the sheet formed by impinging turbulent jets is an obvious process which must be clearly understood before an accurate mechanistic atomization model is developed. The impact waves are particularly important for combustion stability because they determine the temporal nature with which ligaments are shed from the sheet, and thus control the temporal nature of drop formation as well. The wavelength also controls the ligament diameter in conjunction with the thickness of the sheet at its breakup.

The observation that the spacing between these large disturbances is primarily dependent on jet diameter and apparently independent of jet velocity suggests that the source of the impact waves is a long-wave instability on the jet, which also possesses this dependency.[7] This notion is reinforced by the observation of bulges on the free liquid jet prior to impingement that are similar in length to the impact waves. A simple analytical model such as the linear stability model described in Section 2.1.1 cannot accurately give a description of these physical processes. To specifically address the impact wave formation process, modeling efforts have centered on the use of a finite difference Navier-Stokes code[8] (RIPPLE) to investigate the effects of spatial and temporal jet flow oscillations on the primary breakup of the impinging jet fan into ligaments. Directly opposed axisymmetric jets are chosen for study to simplify the analysis.

Representative computational results showing the free surface contour maps of two directly opposed impinging jets are shown in Fig. 4. Harmonic disturbances were imposed on the jets as boundary conditions. The cases presented include imposed sinusoidal disturbances of 250, 500, and 1000 s^{-1} on each jet that are in phase with each other. The imposed disturbance has a radial profile that is proportional to $\sin(\pi r/d_o)$, with the maximum axial velocity oscillation u' at the jet periphery being 5% of the mean jet velocity U_j.

The computed free surface contours have some interesting similarities to directly opposed jets observed in the laboratory. The use of in-phase jet oscillations result in the antisymmetric sheet disturbances that are also seen in the laboratory. The computed movement of disturbances on the liquid sheets has been analyzed for the cases with 500 and 1000 s^{-1} disturbances imposed on the jet; results are provided in Table 2 for the non-dimensionalized disturbance phase speed, c/U, the non-dimensionalized disturbance wavelength, λ/d_o, and the non-dimensionalized disturbance frequency, f_{sheet}/f_{jet}. It is seen that for all cases, the sheet disturbance frequency is equal to the frequency of the imposed oscillation on the jet. Also, the non-dimensional disturbance wavelength for the 500 s^{-1} imposed oscillation case approaches the measured non-dimensional wavelength, which is approximately 2. This model has some promise of clarifying the process of impact wave formation, and ongoing work is focused on the most appropriate way to simulate pre-impingement jet oscillations.

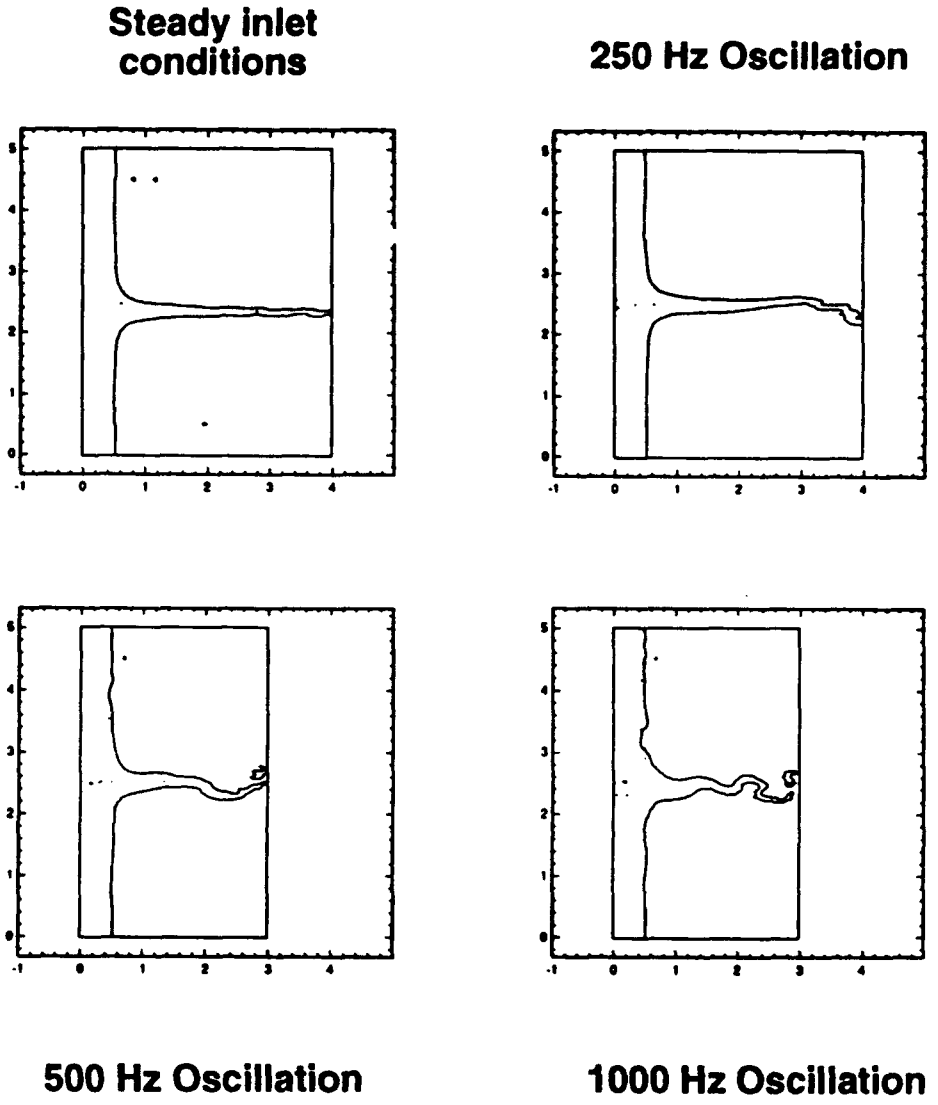

Fig. 4. Computed free surface contours at steady inlet conditions and with harmonic disturbances imposed at the jet inlet. Top jet enters at the upper left hand corner with a mean velocity of -10 m/s and bottom jet enters at the lower left hand corner with a mean velocity of 9.6 m/s. The jet diameter is 10 mm and the imposed disturbances are 5% (maximum) of mean velocity with $\sin(\pi r/2R)$ profile.

Table 2. Summary from Finite-Difference Computations of Unsteady Impinging Jets

Frequency of Imposed Oscillation, Hz	c/U	λ/d_o	f_{sheet}/f_{jet}
500	0.60	1.34	1
1000	0.77	0.78	1

2.2 Experimental Results

A series of detailed measurements and photographic and electronic images were made to characterize the atomization process of two impinging water jets. Both laminar and turbulent jets were studied. The limiting cases of fully-developed laminar and fully-developed turbulent flow were examined. The third limiting case of plug flow was approached by using orifices with an L/d_0 of 5. Some attempts were made to study impinging jets from a sharp-edged orifice, but were cut short because spiraling instabilities on the jets could not be avoided in spite of various means taken to stabilize the flow. Experimental details can be found in References 2 and 3. Table 1 summarizes the test parameters.

For the laminar jets, breakup length and sheet width at breakup were measured from photographs and electronic images for jets emanating from 0.51 mm diameter precision-bore glass tubes for impingement angles of 40, 60, 80, 100, and 180°. Tests were done at open air conditions. The orifice length was 190 mm ($L/d_0 = 375$), resulting in fully-developed laminar flow at the orifice exit. The free jet length prior to impingement was 10 mm. Flow Reynolds numbers from 2800 to 9100 corresponding to jet velocities from 5.5 to 18 m/s were achieved; laminar flow at the higher velocities was possible due to a contoured inlet and the smooth glass tubes. Weber numbers, We_j, varied from 200 to 2200.

Because the practical interest is in turbulent impinging jets, their experimental characterization was much more extensive than it was for laminar impinging jets. The experimental parameters were extended to include effects of orifice diameter, orifice length, free jet impingement length, impingement angle, and jet velocity. Furthermore, to evaluate the effects of practical fabrication techniques, impinging jets from twist-drilled and electro-discharge machined (EDM) orifices were studied in addition to the precision-bore glass tubes. The twist-drilled orifices were 1.0 mm in diameter, 10 mm long, and produced free jets that were 14 mm long prior to impingement. The EDM injector was 0.51 mm in diameter and was 2.5 mm long with a free jet length of 2.5 mm before impingement. For both, the impingement angle was 60°. Measurements included breakup length, sheet width at breakup, the distance between apparent disturbances on the liquid sheet surface, and drop size and drop velocity distributions. For the twist-drilled and EDM injectors, the above measurements were also made in closed chambers at elevated ambient pressures, and under forced oscillatory ambient conditions for the twist-drilled injector.

2.2.1 Atmospheric Pressure Atomization Studies of Impinging Jets from Precision-Bore Glass Tubes

Extensive experimental characterization was made at atmospheric conditions with the precision-bore glass tube injectors for both laminar and turbulent jet conditions to provide a sound basis for later comparisons with data from more practical injector types and for data taken under high-pressure, acoustic, and combusting flow conditions. Most of the glass tube results are detailed in References 2 and 3 and in Appendix 1. A brief summary of the breakup length, drop size distribution, and disturbance wavelength measurements are provided here.

Length measurements of the intact sheet and of periodic structures were made from images such as those shown in Fig. 2. Non-dimensional breakup length, x_b/d_o, is plotted against jet Weber number in Fig. 5 for laminar and turbulent impinging jet cases. Clear differences between the two cases can be seen. The non-dimensional breakup length of the turbulent impinging jets appears to have some dependence on impingement angle, but appears to be relatively independent of jet Weber number. There is a strong dependence on jet Weber number for the laminar impinging jet case.

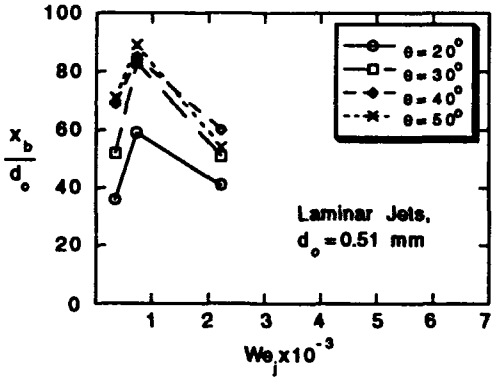

Fig. 5a. Non-dimensional breakup length of laminar impinging jets from precision bore glass tubes as a function of jet Weber number.

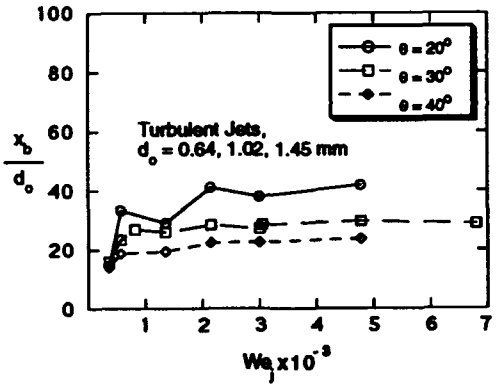

Fig. 5b. Non-dimensional breakup length of turbulent impinging jets from precision bore glass tubes as a function of jet Weber number.

Comparisons of the measured non-dimensional breakup length with predictions from the aerodynamic instability model described in Section 2.1.1 are shown in Fig. 6. Again the differences between the turbulent impinging jet case and the laminar impinging jet case are evident. Laminar impinging jet breakup may be modeled relatively well by the aerodynamic instability model, but again, the turbulent impinging jet breakup shows little dependence on the geometrically scaled jet Weber number. It appears that turbulent impinging jet breakup, which is clearly dependent on orifice diameter and impingement angle, is related to the sheet thickness, which also is determined by orifice diameter and impingement angle .

The measured distance normalized by orifice diameter of the separation between periodic structures for turbulent impinging jets is shown in Fig. 7 as a function of jet velocity. The "wavelength" appears to be primarily dependent on orifice diameter and independent of jet velocity. The observation of independence from jet velocity is contrary to the aerodynamic instability model predictions. The distance between detached ligaments is approximately constant at around 4 orifice diameters, and the distance between surface wave structures is constant at around 2 orifice diameters. There was a rather large spread in the data, with a standard deviation of +/- 35%.

Of course, the combustion process must also be considered in an analysis of combustion instability. In liquid rocket engine combustion, vaporization is the rate-limiting step. The vaporization process is controlled in large by the drop size. Accurate measurements of the drop size distribution are necessary to develop an accurate understanding of the problem of combustion instability. An argon-ion based, two-component Phase Doppler Particle Analyzer (PDPA) was used for making drop size and velocity measurements. A description of the theoretical and operating principles of the PDPA are given elsewhere.[3] Non-dimensional arithmetic mean drop diameters (D_{10}/d_o) are presented in Fig. 8 for the turbulent impinging jet case. A comparison of measured non-dimensional arithmetic mean drop diameter with the monodisperse drop size predicted by the aerodynamic instability model is also shown. The trend of the model predictions match the

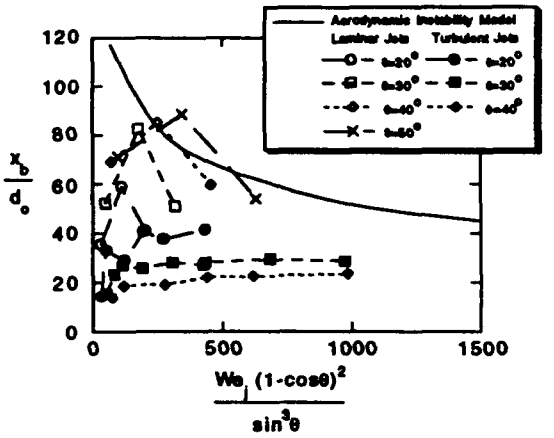

Fig. 6. Non-dimensional breakup length as a function of geometrically scaled jet Weber number. Comparison of measurements with aerodynamic instability model predictions.

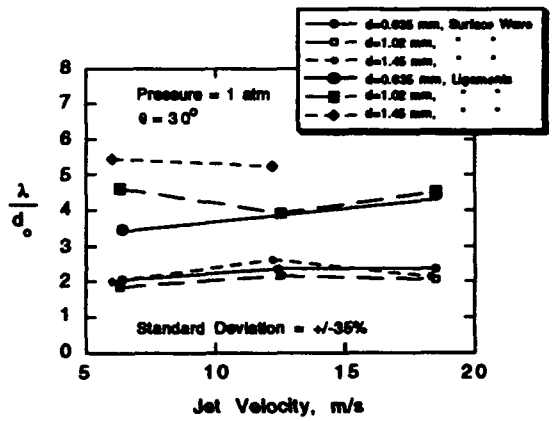

Fig. 7. Non-dimensional distance measured between adjacent surface wave structures and between adjacent ligaments.

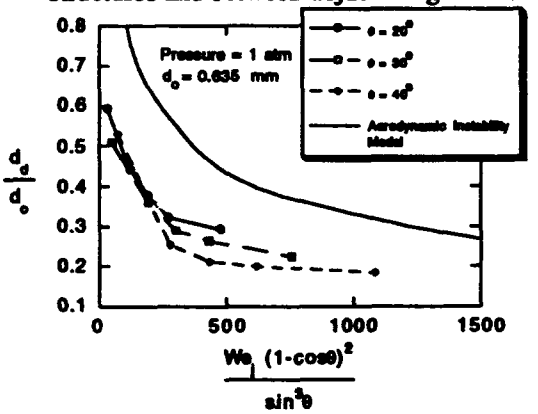

Fig. 8. Non-dimensional drop diameter as a function of geometrically scaled jet Weber number. Comparison of PDPA Measurements with predictions from aerodynamic instability model.

experimental trend quite well, and the measurements appear to collapse into a single curve when plotted against the geometrically scaled jet Weber number as the model predicts. Adjustment to the empirical breakup constant could yield a very good match. However, based on the significant disagreements between prediction and measurement for wavelength and breakup length, the mean drop size agreement is thought to be coincidental.

An empirical correlation for normalized drop size as a function of the geometrically scaled jet Weber number, $We_j f(\theta)$, was obtained with a correlation coefficient of 0.964:

$$\frac{d_D}{d_o} = 2.217 \cdot \{We_j f(\theta)\}^{-0.354} \qquad (5)$$

2.2.2 Effects of Ambient Conditions and Injector Type

Experiments using precision-bore glass tubes provided fully-developed laminar and turbulent jets with well-characterized velocity and turbulence intensity profiles. In practical combustors, however, injection orifices and impingement lengths are short, typically less than 5, and ambient pressures are high and often unsteady. To evaluate these effects, measurements were also taken using twist-drilled and EDM injectors and at high pressure and oscillatory ambient conditions in a transparent acoustic chamber. As with the quiescent, atmospheric pressure case, measurements made within the confines of the acoustic chamber included sheet breakup length and drop size distribution.

Instantaneous images of the EDM injector's spray at 1, 5, and 10 atm ambient pressure are shown in Fig. 9. These images clearly show that faster ligament breakup and drop dispersion result from increases of ambient pressure. A plot of the non-dimensional breakup length, x_b/d_o, as a function of $We_j (=\rho_j v_j^2 d_o/\sigma)$ made from such images is shown in Fig. 10. Each symbol in Fig. 10 represents an average of 17 individual breakup length measurements, while the bars represent the plus/minus standard deviation of those measurements. Reductions in breakup length are seen with increasing ambient pressure. It is also seen that, as for the case of glass tubes at atmospheric ambient conditions, increases in We_j apparently have little effect on the non-dimensional breakup length.

One of the major differences between the glass tubes and the EDM injector is the orifice length-to-diameter ratio, L/d_o. The glass tube L/d_o is 80 while that of the EDM injector is about 5. In spite of the large difference in L/d_o, there is no apparent difference between the measured non-dimensional breakup lengths for the glass tube injector and the EDM injector. This observation that the length-to-diameter ratio does not appreciably affect the impinging jet spray breakup length was also noted by Anderson, et al.[2] Another difference between the two injectors was the length of the free jet prior to impingement: for the glass tube it was 25.4 mm, and for the

EDM injector it was 2.5 mm. Anderson, et al.[2] also noted that free jet length had no apparent effect on spray formation processes of impinging turbulent liquid jets.

(a) (b) (c)

Fig. 9. Instantaneous images of the spray formed by an electro-discharge machined (EDM) impinging jet injector. Orifice diameter was 0.51 mm, and impingment angle was 60°. Ambient pressure was (a) 1 atm; (b) 5.1 atm; (c) 10.5 atm.

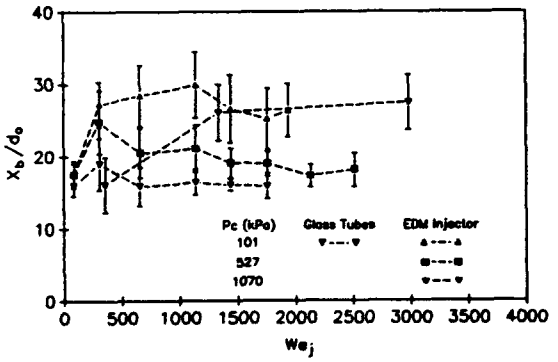

Fig. 10. Non-dimensional breakup length as a function of the jet Weber number, ambient pressure, and injector type.

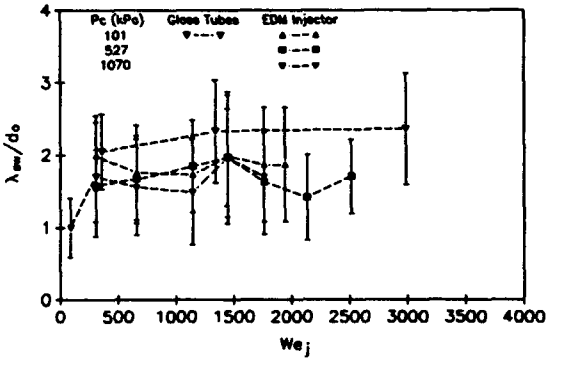

Fig. 11. Non-dimensional surface disturbance wavelength as a function of the jet Weber number, ambient pressure, and injector type.

The effects of ambient pressure and injector type on non-dimensional liquid sheet disturbance wavelength are shown in Fig. 11. A small reduction in disturbance wavelength appears with the EDM injector, which has a substantially smaller orifice length and a substantially smaller free jet length than does the glass tube. However, as with the glass tubes, the non-dimensional disturbance wavelength appears to be essentially independent of velocity, or of jet Weber number as plotted in Fig. 11. The non-dimensional disturbance wavelength also appears to be independent of ambient pressure, at least to 10 atm, which further confirms the inadequacy of the aerodynamic instability model at these conditions.

Drop size data for the EDM injector at atmospheric and higher ambient pressures are compared to glass tube injector drop size data at atmospheric ambient pressure in Fig. 12. A small reduction in non-dimensional drop size is observed for the EDM injector vs the glass tube injector at atmospheric ambient pressure, and another small reduction is observed when the EDM injector is operated at 4.6 atm ambient pressure.

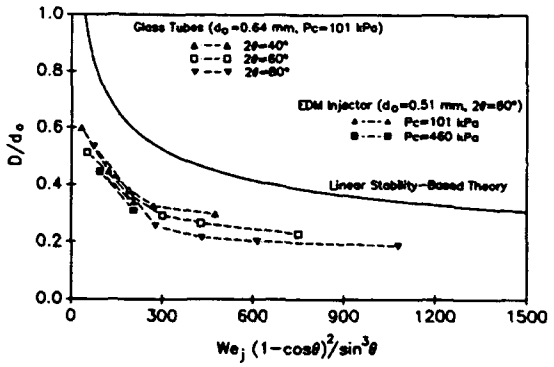

Fig. 12. Non-dimensional arithmetic drop size measured at the impinging jet spray centerline as a function of the geometrically-scaled jet Weber number and injector type. Drop size measurements for the EDM injector were taken at 1 and 4.6 atmospheres.

Together, the data presented in Figs. 10, 11, and 12 can be used to conjecture a partial mechanism for the atomization of liquid sheets formed by impinging jets. The impact waves travel out from the impingement point down the thinning sheet with an undetermined phase speed. Incipient ligament formation occurs due to combined aerodynamic and tensile forces, which accounts for the effect of ambient pressure on breakup length; the impact wave formation process in not considered to be affected by aerodynamic pressure. The ligament then fragments, also under combined aerodynamic and tensile forces. It is not clear why ligament spacing is twice the spacing between adjacent surface disturbances. Although the effect of increased ambient pressure on the ligament fragmentation process is to produce smaller drops, it also results in a shortened breakup length, and thus larger ligaments from the thicker sheet because the impact disturbance wavelength does not change. The net effect is a small change in drop size

due to ambient pressure effects. This phenomenological model is completely consistent with the data shown in Figs. 10, 11, and 12.

The source of the impact waves remains a key question. Because their characteristic length is apparently independent of jet velocity, impingement angle, or ambient pressure, and linearly dependent on jet diameter, it may be postulated that the large impact waves seen on the sheet within a few diameters downstream of the impingement point have their origin in the jet upstream of the impingement point. Instabilities seen on the free jet appear to have a characteristic length that is close to twice the jet diameter, the same as the surface impact waves. It should be noted that helical instabilities on high velocity liquid jets are predicted to have precisely these characteristics, i.e., the fastest growing disturbance has a wavelength approximately equal to twice the jet diameter, and is independent of jet velocity.[7] It is not clear whether there is an interaction mechanism that occurs between the jets. An alternative explanation for the source of the impact waves is that they are generated from oscillations inherent in stagnation point flow.

To examine the effects of an oscillating pressure field, an acoustic chamber (Fig. 13) was designed to excite the first (1W), second (2W) and third (3W) resonant modes at frequencies on the order of several thousand hertz under ambient temperature conditions for air and helium environments. The interior dimensions of the chamber are 254 mm in width, 305 mm in height and 102 mm in depth. Two large Plexiglas faces allow visual access into the chamber, while steel grids brace the Plexiglas for pressurized studies. The maximum chamber pressure is approximately 1.03 MPa (150 psia). These modes and frequencies were chosen because of their similarity to typical rocket instabilities. This frequency range also allows for tests in stable and unstable regions according to the Hewitt stability correlation for realistic injector stability parameter values.

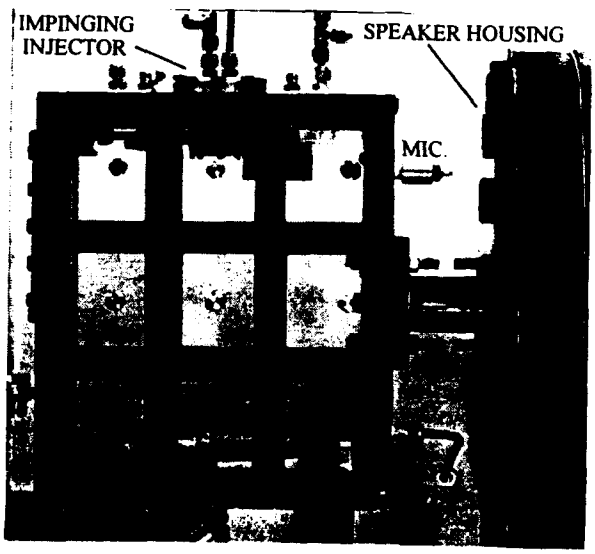

Fig. 13. An image of the transparent acoustic chamber. The interior dimensions of the chamber are 254 mm in width, 305 mm in height, and 102 mm in depth. An acoustic compression driver is encased in a steel cylindrical pressure vessel attached to the right side-wall of the chamber. The impinging jet injector is inserted into the top plate of the chamber.

An acoustic driver with its highest efficiency in the thousand hertz range was attached to the chamber right side-wall and encased in a steel pressure vessel to keep equal pressure across the acoustic driver diaphragm during pressurized experiments. The speaker was driven at a particular frequency and a microphone was used to measure the oscillatory pressure field within the chamber. The twist-drilled or EDM impinging element fit into the top plate of the chamber. Water flowed through a 41.3 mm inner diameter stilling chamber fitted with a sintered brass disc before entering the injector orifices.

To characterize the dimensionality of the applied acoustic field, extensive acoustic measurements were taken at the three resonant modes. The excited 1W, 2W and 3W modes, which had frequencies of 668 Hz, 1362 Hz and 2016 Hz, respectively, were primarily one-dimensional with minor variations in wave amplitude from the top to bottom of the chamber. Fig. 14 shows the measured pressure amplitude as a function of position across the chamber width at atmospheric pressure. The shape of the waveforms are very similar to the expected first through third standing wave modes. All three waveforms were generated with the same input voltage and amplifier gain to the speaker. The peak pressure amplitude for the 2W mode is approximately 3.0 kPa (0.44 psi) at the center of the chamber, and is greater than the other two modes. The maximum observed pressure amplitude is approximately 1.5 kPa (0.22 psi) for the 1W mode and 0.70 kPa (0.10 psi) for the 3W mode.

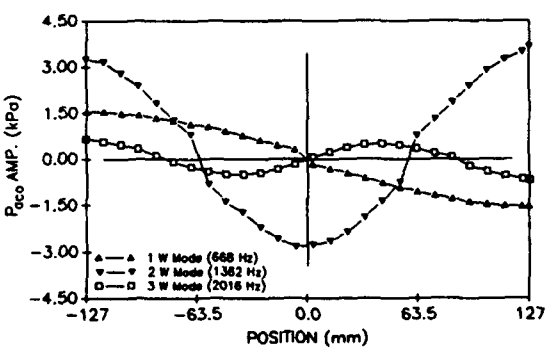

Fig. 14. The measured acoustic pressure amplitude plotted as a function of position along the chamber width for the 1W, 2W, and 3W resonant modes at a chamber pressure of one atmosphere.

The effects on spray formation of oscillating velocity and of oscillating pressure can both be evaluated at the chamber centerline where the injector is located by exciting the 1W and 2W mode, respectively. Since the intended resonant acoustic mode structures are satisfactory, the effects of the applied acoustic field on the impinging jet spray and their relation to the Hewitt stability correlation can be pursued.

Curtains of air across portions of the chamber's Plexiglas walls were used to keep water wetting to a minimum. Breakup length measurements could not be obtained at higher Weber numbers and at higher chamber pressures because of an inability to acquire high contrast images

due to the nature of the turbulent spray as well as lighting problems caused by excessive window wetting. Improvements in window cleaning and lighting practices are needed to make measurements at higher Weber numbers at pressurized conditions.

Drop size and velocity measurements were made using the PDPA along the twist-drilled injector spray centerline which coincides with the chamber centerline at a distance of 25 mm downstream of the impingement point. Axial and transverse (across the chamber width) drop velocities were measured. The injection velocity of the water was 9.0 m/s. Five thousand five hundred valid drop size and velocity samples were obtained at this point for each test condition. The effects of an applied acoustic field were investigated by subjecting the impinging jet spray to the 1W mode at 668 Hz. A pressure node (oscillating velocity) existed at the chamber centerline where the measurements were made. The applied 1W acoustic field did not have an appreciable effect on drop size or drop velocity at the prescribed measurement location for a chamber pressure of one atm, but did, however, noticeably affect the drop formation process at a higher chamber pressure of six atm, i.e., higher ambient densities enhanced the effects of the applied acoustic field. A smaller arithmetic mean drop size, approximately 230 μm, was measured for the acoustically perturbed case, as compared to the quiescent case, where D_{10}= 250 μm. A plot of the drop size number distribution, $f(D)$, versus measured drop diameter, D, for acoustically and non-acoustically perturbed cases is illustrated in Fig. 15. Evident from Fig. 15 is the higher drop number distribution between diameters of 100 to 200 μm for the acoustically perturbed case. This contributes to the observed lower arithmetic mean diameter. Results for the 3W mode were similar to the 1W mode results, whereas the results from an applied 2W mode (pressure anti-node at spray centerline) indicated that oscillating pressure had no apparent effects.

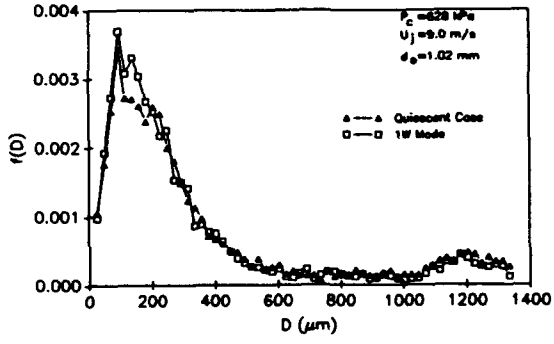

Fig. 15. Drop size number distribution, $f(D)$, measured by the PDPA at 25 mm downstream of the impingement point without and with an applied acoustic field (1W mode). Ambient pressure is approximately 6 atmospheres.

2.2.3 Combusting-Flow Chamber Design

Definitive information regarding combustion instability mechanisms can only be obtained under high-pressure, combusting-flow conditions. Furthermore, it is very desirable to be able to study combustion phenomena under conditions of oscillating pressure fields similar to those that actually occur during a combustion instability event. A high-pressure, optically-accessible combustor in which oscillating pressure fields can be generated has been designed to enable experimental studies under simulated combustion instability conditions at the Cryogenic Combustion Laboratory. Liquid hydrocarbon fuel test capability for impinging jet combusting-flow tests was added to the Cryogenic Combustion Laboratory. A schematic of the chamber is provided in Fig. 16. The short orifice (L/d_o=5), short impingement length (L_{imp}/d_o=5) EDM injector unit that matches practical injector designs and that has undergone cold-flow characterization will be used in the combusting-flow tests.

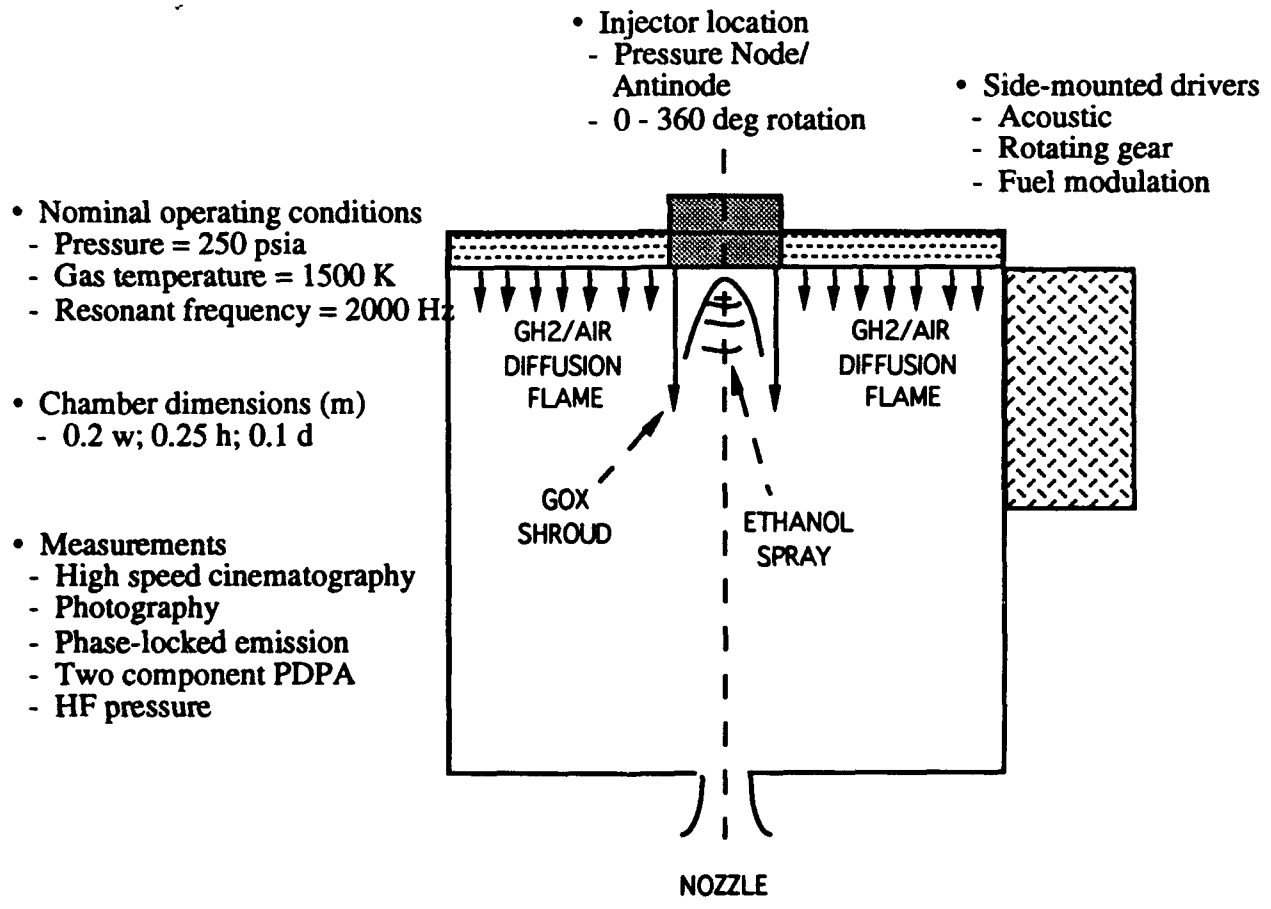

Fig. 16. Schematic of high-pressure, combusting-flow, optically-accessible combustor with features.

2.3 Discussion of Potential Instability Mechanisms

A number of theories and observations have been presented that have attempted to explain the mechanism of combustion instability. A thorough review of past work done in combustion instability was done under this contract, and is summarized in Reference 1. Because the general objective of this work was to develop a rational physical basis for the Hewitt Stability Correlation, the experimental results obtained to date will now be examined in the context of the stability correlation. Specifically, the dependence of breakup length, drop size distribution, and disturbance wavelength (frequency) on d_o/U_j will be examined. It is important to keep in mind that the discussion to follow pertains to cold-flow atomization data, and that, ideally, the functional dependence of the impinging jet atomization characteristics should be evaluated under actual rocket conditions. To aid understanding the discussion to follow, it is useful to remember than an increase in the stability parameter, d_o/U_j, leads to an increase in stability.

The functional dependence of the measured breakup length for the glass tube injector on the impingement angle and d_o/U_j is shown in Fig. 17 for an orifice diameter of 0.64 mm. For all impingement angles, the nondimensional quantity, x_b/d_o, decreases with increasing d_o/U_j. Similar behavior is noted for different orifice diameters, as displayed in Fig. 18; however, with an increase in orifice diameter, the nondimensional breakup length is less sensitive to variations in d_o/U_j. The trend of the measured breakup length as a function of chamber pressure and injector stability parameter is shown in Fig. 19 for the EDM injector (d_o=0.51 mm). Under

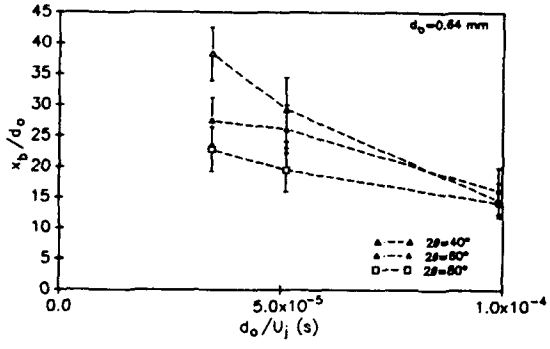

Fig. 17. Non-dimensional breakup length of liquid sheet formed by impinging jets from glass tubes as a function of stability parameter and impingement angle.

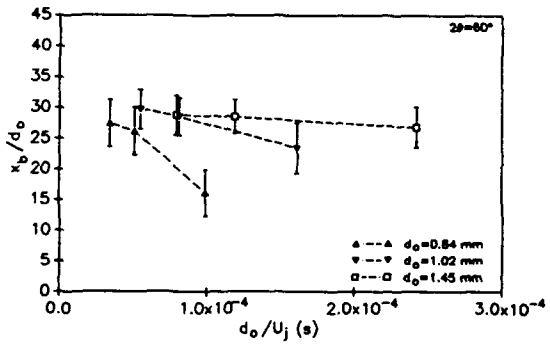

Fig. 18. Non-dimensional breakup length of liquid sheet formed by impinging jets from glass tubes as a function of stability parameter and orifice diameter.

atmospheric pressure (P_c=101 kPa), the nondimensional breakup length initially increases then decreases with increasing d_o/U_j. With increasing chamber pressure, the nondimensional breakup length seems less sensitive to changes in d_o/U_j. By itself, the observation that breakup length decreases with increasing d_o/U_j is not consistent with the notion that engine stability increases with an increase in the injector stability parameter. A reduction in sheet breakup length most likely moves the combustion zone closer to the injector face plate, thus increasing the probability of the initiation of instability phenomena. It should be noted however that the sheet breakup length stays approximately constant with increasing d_o/U_j at higher ambient pressures as shown in Fig. 19.

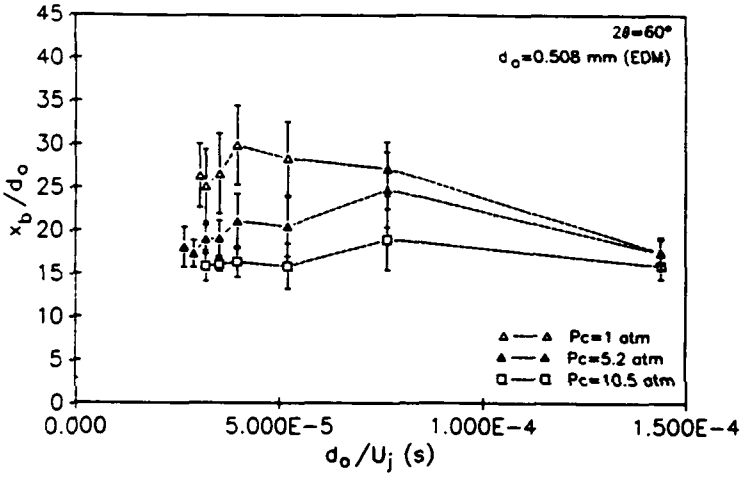

Fig. 19. Non-dimensional breakup length of liquid sheet formed by impinging jets from EDM injector as a function of stability parameter and ambient pressure.

The mean drop size and the distribution of drop size may be critical in terms of whether instability will ensue. Figure 20 shows the non-dimensional arithmetic mean diameter, D_{10}/d_o, along the spray centerline at an axial location of 41 mm from the impingement point, plotted as a function of d_o/U_j and 2θ. Note that the orifice diameter is constant, so changes in d_o/U_j result only from the variation in jet velocity. An increase in mean drop size is noted with increasing d_o/U_j, thus leading to the conclusion that bigger drops have a stabilizing effect, which has been widely suggested, but never substantiated.[1] Similar mean drop size trends with d_o/U_j are observed for different orifice diameters and at different locations in the spray field. It should be noted that the same mean drop size will not necessarily be obtained for any given value of d_o/U_j.

Another important consideration is the degree of polydispersity of the drop size distribution. It is reasonable to expect that stability will be enhanced if there is a wide distribution of drop sizes because any present effects of resonant burning can be essentially neutralized by different-sized drops that release most of their chemical energy out of phase with the drops that are burning in resonance with pressure oscillations. Conversely, in the case of a

relatively monodisperse drop distribution, the drops will burn similarly, i.e., have a similar drop lifetime. The number distribution, $f(d_D)$, plotted as a function of drop size, d_D, and the injector stability parameter is shown in Fig. 21. The measured distributions were taken along the spray centerline (x=0) at an axial location (z) of 41 mm for an injector orifice diameter of 0.64 mm and an impingement angle of 60°. The change in d_o/U_j was obtained here by changing jet velocity while maintaining orifice diameter. Notice that an increase in the injector stability parameter leads to broader distributions with larger mean values. Similar distribution shapes are observed for different radial positions and impingement angles for a given orifice diameter.

Changes in the stability parameter can also be realized by changing d_o. Eight number distributions as a function of d_D and d_o/U_j are shown in Fig. 22 for two different injectors. The hollow symbols represent data from the 0.64 mm diameter glass tube injector and the solid symbols represent data from the 1.45 mm diameter glass tube injector. All the data was acquired along the spray centerline and at a similar non-dimensional axial location. Once again, an increase in d_o/U_j - this time obtained via a combination of changes in d_o and U_j - leads to broader and flatter distributions with a corresponding increase in mean drop size.

Finally, it is clear that periodic drop formation could lead to periodic burning and subsequent instability if the frequency with which the drops entered the combustion zone matched in some fashion some resonant frequency of the chamber. Disturbance wavelength data was converted to atomization frequency simply by dividing the jet velocity by the measured wavelength; the assumption that the disturbance velocity is equal to the sheet velocity needs to be substantiated. Earlier studies[2] showed that measured drop velocities, and therefore the sheet velocity, were nearly equal to the jet velocity. Atomization frequency data is presented in Fig. 23 based on ligament spacing. The trend of atomization frequencies are quite similar to the maximum possible combustion instability frequency given by the Hewitt Stability Correlation, also shown in Fig. 23. The similar dependencies of maximum possible instability frequency and atomization frequency on d_o/U_j is significant in terms of primary atomization being a key process in combustion instability. The calculated atomization frequency is about two times greater than the maximum combustion instability frequency as predicted by the stability correlation, however. The effects of periodic atomization must be more carefully analyzed, and the atomization frequency must still be determined under high pressure, combusting-flow conditions. There must also be an accounting for the effects of drop size distribution as shown in Figs. 21 and 22.

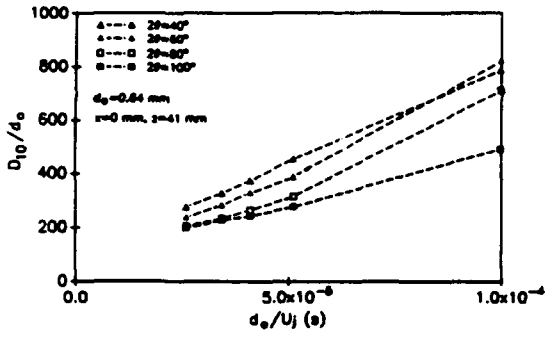

Fig. 20. Non-dimensional arithmetic mean drop size of spray formed by turbulent impinging jets from glass tubes as a function of stability parameter and impingement angle.

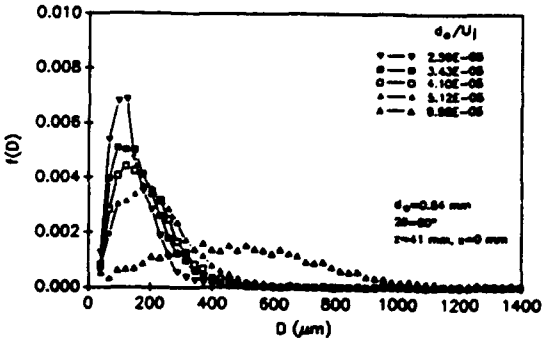

Fig. 21. Number distribution of drop sizes in spray formed by turbulent impinging jets from glass tubes as a function of the stability parameter.

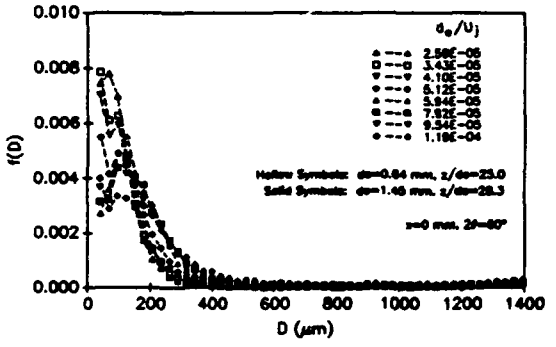

Fig. 22. Number distribution of drop sizes in spray formed by turbulent impinging jets from glass tubes as a function of the stability parameter. Data from two different injectors are shown.

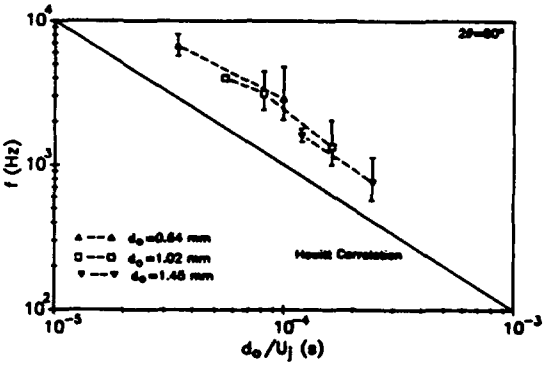

Fig. 23. Atomization frequency of spray formed by turbulent impinging jets from glass tubes as a function of stability parameter. Frequency is assumed to be equal to the ratio of sheet speed to distance between adjacent detached liquid ligaments. Also shown is maximum instability frequency predicted by the stability correlation.

3.0 SUMMARY

The most complete and systematic study of the atomization of impinging liquid jets to date has been completed under this contract. Effects of jet flow condition, orifice diameter, impingement angle, pre-impingment length, fabrication procedure, and jet velocity at steady and oscillating, and atmospheric - and high - pressure conditions have been investigated. Results of these experimental studies have been compared to current theories in terms of sheet breakup length, wave structure, and drop size. Experiments contrasting laminar and turbulent jet conditions clearly demonstrate that the jet conditions have a dramatic effect on the atomization process. Specifically, the measured breakup lengths for laminar impinging jets are longer and displayed different trends as a function of jet velocity and impingement angle than those for turbulent impinging jets. In addition, the measured spray width for the turbulent impinging jet case remained approximately constant as a function of jet velocity and impingement angle for a fixed orifice diameter, unlike the laminar impinging jet case. The present results are generally in agreement with earlier studies at atmospheric pressure by Dombrowski and Hooper,[10] however, there are important discrepancies with their speculation that these differences are due to velocity profile differences between fully-developed laminar flow and fully-developed turbulent flow; implicit in their reasoning was the assumption that aerodynamic forces played a large role in the formation of the impact waves . Based on the observations in our laboratory, it appears more likely that large pressure and momentum fluctuations in the liquid, that are accentuated near the impingement point and have their origins in long wave instabilities that are present on the jet prior to impingement, determine the breakup characteristics of turbulent impinging jets, and are responsible for the obvious differences between laminar and turbulent cases. A quantitative assessment of the specific mechanisms controlling atomization remains to be established.

Comparisons of the experimental results were also made with results from a linear stability-based theory. The model predicted a monotonically decreasing sheet breakup length with increasing Weber number which is opposite to the trend observed for turbulent impinging jets. Thus, the use of the aerodynamic instability model for describing sheet breakup appears to be incorrect, at least for the conditions of these studies. Results from computations from a finite-difference Navier-Stokes model were also compared to the experimental data and interesting similarities between the predicted and measured values of disturbance wavelength were observed. Measurements of disturbance phase speed must be made for further corroboration of the model.

Measurement of surface wave and periodic ligament formation phenomena for turbulent impinging jets indicates that the observed wavelengths are directly proportional to the orifice diameter and independent of jet velocity and impingement angle, which is also contrary to results from the linear stability model that predicts a strong dependence of these variables on jet

velocity. It is interesting, however, that the aerodynamic instability model does provide quite a reasonable predictive capability for drop size. Measurements made in a high-pressure acoustic chamber indicate that there are some effects of ambient pressure at greater than atmospheric pressure. Based on the results of the above studies, approaches to modeling impinging jet atomization should continue to focus on pre-impingement jet conditions and the physics near the jet impingement point, specifically the source of the observed impact waves that appear to control turbulent impinging jet breakup.

The experimental results were studied in the context of the Hewitt Stability Correlation. At the conclusion of these cold-flow studies, three observations with potentially high significance can be made:

(1) The frequency with which periodic surface waves and ligament structures are formed have a marked similarity to the highest possible combustion instability frequency as predicted by the stability correlation.

(2) Increases in the value of the stability parameter, indicating increased stability margin, coincide with an increase in measured mean drop size.

(3) Increases in the value of the stability parameter also coincide with a increase in polydispersity of the drop size distribution.

Each of these observations are consistent with a reasonable theory of combustion instability.

Combustion measurements at realistic chamber and injector conditions are critical to defining combustion instability mechanisms. A design of an optically-accessible combustion chamber has been developed. The first chamber will be designed for 250 psi chamber pressure. Pressure oscillations will be introduced into the chamber to simulate a combustion instability event. Injector elements will be placed strategically to allow the discrimination of oscillatory pressure effects from oscillatory velocity effects. Ethanol will be used as the liquid fuel. Measurements will be phase-locked to the pressure oscillations, and will include combustion light measurements (OH or CH radical emission) and drop size and velocity measurements. A combustion response model will be used to analyze the combustion test results. Unsteady atomization and drop distribution effects will be accounted for in the analysis.

4.0 REFERENCES

[1] Anderson, W. E., Ryan, H. M., and Santoro, R. J., "Combustion Instability of Importance to Liquid Bi-Propellant Rocket Engines," 28th JANNAF Combustion Meeting, San Antonio, TX, Oct. 28 - Nov. 1, 1991.

[2] Anderson, W. E., Ryan, H. M., Pal, S., and Santoro, R. J., "Fundamental Studies of Impinging Liquid Jets," AIAA paper 92-0458, 30th Aerospace Sciences Meeting, Reno, NV, Jan. 6 - 9, 1992.

[3] Ryan, H. M., Anderson, W. E., Pal, S., and Santoro, R. J., "Atomization Characteristics of Impinging Liquid Jets," AIAA paper 93-0230, 31st Aerospace Sciences Meeting, Reno, NV, Jan. 11 - 14, 1993 (accepted for publication in Journal of Propulsion and Power).

[4] Couto, H. S. and Bastos-Netto, D., "Modeling Drop Size Distribution from Impinging Jets," J. Propulsion, July-August 1991, pp. 654-656.

[5] Dombrowski, N. and Johns, W. R., "The Aerodynamic Instability and Disintegration of Viscous Liquid Sheets," Chem. Eng. Science, Vol. 18, 1963, pp. 203-214.

[6] Brodkey, R. S., Phenomena of Fluid Motions, Addison-Wesley Series in Chemical Engineering, 1967.

[7] Levich, V.G., Physicochemical Hydrodynamics, Prentice Hall, 1962.

[8] Kothe, D.B., Mjolsness, R.C., and Torrey, M.D., "RIPPLE: A Computer Program for Incompressible Flows with Free Surfaces," LA-12007-MS, Los Alamos National Laboratory, Los Alamos New Mexico, 87545.

[9] Heidmann, M. F., Priem, R. J. and Humphrey, J. C., "A Study of Sprays Formed by Two Impinging Jets," NACA Technical Note 3835, March 1957.

[10] Dombrowski, N. and Hooper, P. C., "A Study of the Sprays Formed by Impinging Jets in Laminar and Turbulent Flow," J. Fluid Mechanics, Vol. 18, Part 3, 1963, pp. 392-400.

5.0 PUBLICATIONS

1. Anderson, W. E., and Santoro, R. J., "Primary Atomization Mechanisms of Impinging Jet Injectors," First Annual Symposium on Liquid Rocket Engine Combustion Instability, University Park, PA, Jan. 18 - 20, 1993 (accepted for publication in AIAA Progress Series on Liquid Rocket Engine Combustion Instability).

2. Ryan, H.M., Anderson, W.E., Pal, S., and Santoro, R.J., "Atomization Characteristics of Impinging Liquid Jets," AIAA paper 93-0230, 31st Aerospace Sciences Meeting, Reno, NV, Jan. 11 - 14, 1993 (to be published in Journal of Propulsion and Power, Vol 11, No. 1, 1995).

3. Ryan, H.M., Anderson, W.E., Pal, S., and Santoro, R.J., "Spray Formation Processes of Impinging Jet Injectors," Propulsion Engineering Research Center Fifth Annual Symposium, The Pennsylvania State University, University Park, PA, Sept. 8 - 9, 1993.

4. Ryan, H.M., Anderson, W.E., Pal, S., and Santoro, R.J., "Combustion Instability Phenomena of Importance to Liquid Propellant Engines," Propulsion Engineering Research Center Fourth Annual Symposium, Marshall Space Flight Center, Huntsville, AL, Sept. 9 - 10, 1992.

5. Anderson, W.E., Ryan, H.M., Pal, S., and Santoro, R.J., "Fundamental Studies of Impinging Liquid Jets," AIAA paper 92-0458, 30th Aerospace Sciences Meeting, Reno, NV, Jan. 6 - 9, 1992.

6. Hoover, D.V., Ryan, H.M., Pal, S., Merkle, C.L., Jacobs, H.R., and Santoro, R.J., "Pressure Oscillation Effects on Jet Breakup," Heat and Mass Transfer in Spray Systems, C. Presser and A.K. Gupta (eds.), HTD-Vol. 187, The American Society of Mechanical Engineers, New York, 1991, pp. 27 - 36.

7. Anderson, W.E., Ryan, H.M., and Santoro, R.J., "Combustion Instability of Importance to Liquid Bi-Propellant Rocket Engines," 28th JANNAF Combustion Meeting, San Antonio, TX, Oct. 28 - Nov. 1, 1991.

8. Santoro, R.J., "A Summary of The JANNAF Workshop on Diagnostics", 28th JANNAF Combustion Subcommittee Meeting, San Antonio, TX, Oct. 28 - Nov. 1, 1991.

6.0 PARTICIPATING PROFESSIONALS

Professor Robert J. Santoro, Professor of Mechanical Engineering

Mr. William E. Anderson, Graduate Student, Department of Mechanical Engineering

Mr. Harry M. Ryan, Graduate Student, Department of Mechanical Engineering

Mr. Shamim Rahman, Graduate Student, Department of Mechanical Engineering

Mr. Steven Thambam, Graduate Student, Department of Mechanical Engineering

Dr. Sibtosh Pal, Research Associate, Department of Mechanical Engineering

Mr. Ecton English, Visiting Undergraduate Student, Department of Mechanical Engineering, University of Maryland

Mr. Larry Schaaf, Engineering Assistant, Department of Mechanical Engineering

7.0 MEETINGS AND PRESENTATIONS

1. Ryan, H.M., Anderson, W.E., Pal, S., and Santoro, R.J., "Spray Formation Processes of Impinging Jet Injectors," Propulsion Engineering Research Center Fifth Annual Symposium, The Pennsylvania State University, University Park, PA, Sept. 8 - 9, 1993.

2. Anderson, W.E., Ryan, H.M., Pal, S., and Santoro, R.J., "Impinging Jet Injectors," CFD Consortium, Marshall Space Flight Center, Huntsville, AL, October 28 - 29, 1993.

3. Anderson, W. E., and Santoro, R. J., "Primary Atomization Mechanisms of Impinging Jet Injectors," First Annual Symposium on Liquid Rocket Engine Combustion Instability, University Park, PA, Jan. 18 - 20, 1993.

4. Ryan, H.M., Anderson, W.E., Pal, S., and Santoro, R.J., "Atomization Characteristics of Impinging Liquid Jets," 31st Aerospace Sciences Meeting, Reno, NV, Jan. 11 - 14, 1993

5. Ryan, H.M., Anderson, W.E., Pal, S., and Santoro, R.J., "Combustion Instability Phenomena of Importance to Liquid Propellant Engines," Propulsion Engineering Research Center Fourth Annual Symposium, Marshall Space Flight Center, Huntsville, AL, Sept. 9 - 10, 1992.

6. Anderson, W.E., Ryan, H.M., Pal, S., and Santoro, R.J., "Fundamental Studies of Impinging Liquid Jets," 30th Aerospace Sciences Meeting, Reno, NV, Jan. 6 - 9, 1992.

7. Hoover, D.V., Ryan, H.M., Pal, S., Merkle, C.L., Jacobs, H.R., and Santoro, R.J., "Pressure Oscillation Effects on Jet Breakup," 1991 ASME Winter Annual Meeting, Atlanta, GA, Dec. 1 - 6, 1991.

8. Anderson, W.E., Ryan, H.M., and Santoro, R.J., "Combustion Instability of Importance to Liquid Bi-Propellant Rocket Engines," 28th JANNAF Combustion Meeting, San Antonio, TX, Oct. 28 - Nov. 1, 1991.

9. Santoro, R.J., "A Summary of The JANNAF Workshop on Diagnostics", 28th JANNAF Combustion Subcommittee Meeting, San Antonio, TX, Oct. 28 - Nov. 1, 1991.

8.0 INTERACTIONS

Throughout this research effort, extensive interactions with a number of personnel from Aerojet Propulsion Division of Sacramento, CA, have occurred. These interactions have primarily involved Messrs. Jerry Pieper, James Hulka, and Ross Hewitt. Specific interactions with Aerojet have been:

(1) Aerojet has provided uni-element impinging jet injectors representative of the XLR-132, Transtage, and F-1 engines for study.

(2) W. Anderson and S. Pal visited Aerojet in January, 1992 to discuss the initial program plan and present research capabilities at Penn State.

(3) R.J. Santoro, S. Pal, and S. Rahman visited Aerojet in December, 1992 to present results from this and associated studies.

(4) R. Hewitt visited Penn State on July 23 and 24, 1992 to review acoustic chamber and study injector element designs.

(5) J. Pieper visited Penn State in October, 1993 to review research results and combustion experiment plans, and to provide an overview of current propulsion programs and associated design issues.

(6) W. Anderson visited Aerojet on June 10, 1994 to present results and review research plans.

Additional interactions have occurred with engineers from the Rocketdyne Division of Canoga Park, CA, specifically Mr. Steve Fisher and Dr. Robert Jensen. Rocketdyne has provided support, under a separate contract, to demonstrate the measurement technique for obtaining drop size and velocity distributions produced by impinging jet injectors under high pressure and combusting conditions. These experiments were successfully performed at the Penn State Cryogenic laboratory by Dr. Robert Santoro and his research staff and students in 1994, and the results were transmitted to Rocketdyne.

APPENDIX 1

Atomization Characteristics of Impinging Liquid Jets

H.M. Ryan, W.E. Anderson, S. Pal, and R.J. Santoro

to be published in Journal of Propulsion and Power, Vol. 11, No. 1, 1995

In Print. Tentative Issue:
Journal of Propulsion and Power,
Vol. 11, No. 1, Jan.-Feb. 1995.

Atomization Characteristics of Impinging Liquid Jets

H.M. Ryan, W.E. Anderson, S. Pal and R.J. Santoro

Propulsion Engineering Research Center

and

Department of Mechanical Engineering

The Pennsylvania State University

University Park, PA 16802

Abstract

The atomization characteristics of sheets formed by both laminar and turbulent impinging jets were experimentally studied as a function of flow and injector geometric parameters. In particular, sheet breakup length along the sheet centerline, distance between adjacent waves apparent on the sheet, and drop size distributions were measured over a Weber number range between 350 to 6600 and a Reynolds number range between 2800 to 26000. A linear stability-based model was used to determine the most unstable wavenumber and the corresponding growth rate factor on two-dimensional thinning inviscid and viscous sheets. These wave characteristics were used to predict both the sheet breakup length and the resulting drop sizes. A second model, applicable for a low Weber number regime, in which sheet disintegration is controlled by stationary antisymmetric waves, was used to predict the shape of the sheet formed by two impinging liquid jets. The linear stability-based theory predictions of breakup length did not agree in trend or magnitude with experimental measurements. However, for Weber numbers less than 350, the measured breakup length for laminar impinging jets was within 50% of that predicted by the stationary antisymmetric wave-based model. Finally, drop size predictions based on linear stability theory agreed in trend but not in magnitude with the measured drop sizes. The contrast between the sheet

atomization characteristics of laminar versus turbulent impinging jets suggest that the initial conditions of the impinging jets significantly influence the sheet breakup mechanism. Also, the comparison between experimental results and theoretical predictions indicates that the impact wave generation process at the jet impingement point needs to be incorporated in the theoretical models for sheet atomization.

Nomenclature

English Symbols

d	diameter
F	thickness distribution
h	sheet thickness
k	wavenumber
l	length
L	length of injection element
r	radial distance from impingement point
Re	Reynolds number ($=U_j d_o/\nu_l$) based on liquid properties, jet velocity, and orifice diameter
Re_s	Reynolds number ($=U_s h/\nu_l$) based on liquid properties, sheet velocity, and sheet thickness
s	ratio of gas density to liquid density
t	time
U	velocity
W	maximum width of sheet
We	Weber number ($=\rho_l U_j^2 d_o/\sigma$) based on liquid properties, jet velocity and orifice diameter
We_s	Weber number ($=\rho_l U_s^2 h/\sigma$) based on liquid properties, sheet velocity and sheet thickness
x	axial distance from impingement point
y	coordinate perpendicular to x in the plane of the sheet

Greek Symbols

α	fan inclination angle
β	complex growth rate factor ($\beta=\beta_r+i\beta_i$)
η	disturbance amplitude
λ	wavelength
μ	dynamic viscosity
ν	kinematic viscosity
π	pi (=3.14159)
ϕ	angular coordinate on sheet
ρ	density
θ	impingement half-angle
σ	surface tension

Subscripts

10	arithmetic
30	volume
b	breakup
D	drop
e	edge
g	gas
i	imaginary
j	jet
l	liquid
L	ligament
m	maximum

nd nondimensional

o orifice or initial

r real

s sheet

sw surface wave

Introduction

Impinging jet injectors are commonly used in many rocket engines, prominent examples being the F-1, H-1, Titan and XLR-132.[1] Furthermore, laser-drilled micro-orifice doublet impinging jet injectors have recently received attention due to their potential low cost and high efficiency.[2] Impinging jet injectors are most often used with RP-1/liquid oxygen (LOX) and nitrogen tetroxide (NTO)/monomethyl hydrazine (MMH) propellant combinations.[3] The relative ease of fabrication of impinging jet injectors also makes this type of injector an attractive alternative to coaxial injector elements typically used for LOX/H_2 engines. Currently, no mechanistic design analysis method exists for this common type of injector.

A schematic diagram of a typical like-on-like impinging jet injector and the resultant spray is shown in Fig. 1. The individual impinging jet injector elements are fed propellant through a manifold. The inlets are usually sharp edged; hence the flow detaches from the wall to form a *vena contracta*. The flow typically reattaches to the wall and exits into the chamber. The two emerging cylindrical jets impinge at a point with an impingement angle of 2θ, which is typically about 60°. The Reynolds number, Re ($=U_j d_o/\nu_l$), and Weber number, We ($=\rho_l U_j^2 d_o/\sigma$), based on liquid properties, jet velocity, and orifice diameter are on the order of 10^5-10^6 under rocket conditions. The length-to-diameter ratio (L/d_o) of the orifice and the pre-impingement length-to-orifice-diameter ratio (l_j/d_o) are both typically between three and ten. The symbol o shown in Fig. 1 is the angular coordinate in the plane of the sheet.

The impinging liquid jets form a sheet in a plane perpendicular to the plane of the jets, and the sheet is usually canted at an angle, α, from the normal to the injector faceplate to improve mixing.

The impetus behind understanding the atomization mechanism(s) of impinging jet injectors is the direct effect atomization has on subsequent combustion processes, and the established link between atomization and combustion instability phenomena.[1,3,4] Previous cold flow[1-8] and hot-fire[3] experimental studies of impinging jet atomization have typically involved changing the injector geometry and flow properties and recording the effect of these changes on the resultant spray. Visualizations of impinging jet sprays under both cold flow and hot-fire conditions indicate that the sheet breaks up in a periodic manner into ligaments, which subsequently disintegrate into drops.[3] Previous studies have shown that the sheet structure, ligament/drop formation frequency and drop size are all sensitive to the injector design and operating parameters.[4] In addition, researchers have modeled the breakup behavior of impinging jets with varying degrees of complexity and success.[6-9] However, a fundamental understanding of the atomization mechanism(s) still does not exist.

In this study, measurements of sheet breakup length, and surface wave and periodic ligament separation characteristics made from instantaneous images of the impinging jet spray, and drop size measurements within the spray field, are presented. These results are compared to predictions made with current modeling approaches, and with earlier experimental studies. Similar to previous workers,[5] the effects of laminar versus turbulent jet conditions on the spray breakup process have been studied over a Weber number range between 350 to 6600 and a Reynolds number range between 2800 to 26000. The objectives of the current study are to extend and confirm previous experimental work on impinging jet atomization and to provide a firm basis from which to address combustion instability phenomena associated with this type of injector. To aid in the comparison of current work with previous studies, a review of previous theoretical and experimental work on liquid sheet breakup is presented next.

Theoretical Models of Liquid Sheet Breakup

The study of atomization characteristics associated with many injector types often involves analyzing the breakup behavior of liquid sheets. There have been a number of theoretical studies of the general case of liquid sheet atomization,[10-20] as well as the atomization of a sheet formed by two impinging jets.[7-9] Models of liquid sheet atomization can be subdivided into numerical[10-12] and analytical treatments[13-20] based on the growth of infinitesimal disturbances due to aerodynamic stresses on the liquid sheet surface. The analytical models typically involve linear wave growth, while the numerical studies examine nonlinear wave growth. In a different approach, Childs and Mansour[10] used a Navier-Stokes method and a Lagrangian scheme to track the liquid-gas interface to provide an argument that boundary layer effects in both the liquid and gas phases enhance the wave growth rate for wind induced instabilities. These analytical and numerical studies provide insight into the important physical processes causing liquid sheet disintegration, and predict physical quantities, such as drop size, which compare relatively well with observations made in appropriate experimental studies. However, the application of linear and nonlinear wave growth based models to the case of sheets formed by two impinging jets has not been thoroughly investigated. Anderson *et al.*[8] adapted linear stability theory to the case of impinging jet atomization, while Ibrahim and Przekwas[9] extended Taylor's[7,19] work to predict the sheet shape at low Weber numbers. A review of linear stability theory for liquid sheet atomization applicable for high Weber number impinging jets, as well as Ibrahim and Przekwas'[9] sheet shape model for low Weber number impinging jets is discussed next.

Linear stability theory based on the growth of infinitesimal disturbances due to aerodynamic stresses on the liquid sheet surface has been used to describe the disintegration of liquid sheets.[13-18] The disturbance on the sheet surface, η, is given by

$$\frac{\eta}{\eta_o} = e^{\beta_i t} \tag{1}$$

where η_o is the initial displacement amplitude, β_i is the growth rate and t is time.

Typically the growth rate, β_i, is calculated for a spectrum of wavenumbers, k. The disturbance wavenumber, k_m, corresponding to the maximum growth rate, $\beta_{i,m}$, controls the breakup process. Both sinuous (antisymmetric) and dilatational (symmetric) waves can grow; however, previous research indicates that sinuous waves grow faster than dilatational waves,[13] hence only the behavior of sinuous disturbances are considered hereafter. The theory does not predict a critical disturbance amplitude for sheet disintegration, and consequently, an empirical relation of the following form is used:[14]

$$\int_0^{t_b} \beta_{i,m} dt = \int_0^{x_b} \frac{\beta_{i,m}}{U_s} dx = 12 \tag{2}$$

where t_b is the sheet breakup time, x_b is the breakup distance and U_s is the sheet velocity. Thus, through the above empirical equation, the length of the intact sheet can be determined once a relation for the maximum growth rate, $\beta_{i,m}$, is ascertained. The wavenumber, k_m, associated with the fastest growing disturbance is used to subsequently predict the size of ligaments and drops shedding from the edge of the intact sheet.[14]

The derivation of an expression for the growth rate factor and the wavenumber has been done for an inviscid constant thickness sheet,[13] and an attenuating viscous sheet.[14,15] Other researchers have extended these equations describing sheet breakup to the case of the sheets formed by impinging jets.[8,9] A concise summary of the appropriate equations and their underlying assumptions is given next.

Squire[13] investigated the growth of antisymmetric disturbances for constant thickness, inviscid liquid films, and derived expressions for the wavenumber and corresponding growth rate coefficient for the most unstable wave. The wavenumber, k_m, for the most unstable wave was given as

$$k_m = \frac{\rho_g U_s^2}{2\sigma} \tag{3}$$

where ρ_g is the gas density and σ is the surface tension. The corresponding maximum growth rate factor was given by

$$\beta_{i,m} = \frac{\rho_g U_s^2}{\sqrt{2\rho_l \sigma h}} \tag{4}$$

where ρ_l is the liquid density and h is the sheet thickness. The above two relations are valid for $We_s (=\rho_l U_s^2 h/\sigma) > 1$, and for disturbance wavelengths large compared to the sheet thickness. Squire[13] compared his predictions of the wavelength of the most unstable disturbance, λ_m $(=2\pi/k_m)$, to those measured from photographs of liquid sheets produced by a nozzle, and showed, in general, good agreement.

Dombrowski and Johns[14] extended Squire's[13] analysis by including the effects of viscosity and a diminishing sheet thickness in analyzing the disintegration of two-dimensional liquid sheets through aerodynamic instability. By considering a force balance on the liquid between pressure, surface tension, viscous and inertial forces, they developed an equation relating the disturbance wavenumber and the growth rate factor to fluid and sheet parameters.[14] Brodkey[21] rewrote Dombrowski and John's[14] general dispersion equation in a clearer form:

$$\beta_{i,nd}^2 + \frac{(kh)^2}{Re_s}\beta_{i,nd} + \frac{2(kh)^2}{We_s} - 2skh = 0 \tag{5}$$

where

$$\beta_{i,nd} = \frac{\beta_i h}{U_s}, \quad Re_s = \frac{U_s h}{\nu_l}, \quad We_s = \frac{\rho_l U_s^2 h}{\sigma}$$

where ν_l is the liquid viscosity and s is the ratio of the gas density to the liquid density. In the above equation, the first term represents the rate of change of momentum of a liquid element; the second term arises because of viscous effects; the third term represents the effect of surface forces; and the fourth term, the effect of aerodynamic forces.

Weihs,[15] like Dombrowski and Johns,[14] stated that Kelvin-Helmholtz aerodynamic instabilities resulted in the breakup of a thin, viscous liquid sheet. However, Weihs[15] derived a general solution for the shape of the sheet by employing hypergeometric functions, which was subsequently simplified to

apply to the far field region (i.e. far from the nozzle, or the impingement point in this case) where changes in sheet thickness are negligible. He obtained the following equation for the growth rate factor:

$$\beta_i = \frac{\nu_l k^2}{2}\left[-1+\sqrt{1+\frac{8(\rho_g k U_s^2-\sigma k^2)}{\nu_l^2 k^4 \rho_l h}}\right] \tag{6}$$

The same equation for the growth rate factor is obtained by reducing Dombrowski and Johns'[14] general dispersion equation (Eq. 5).

Equation 6 relates the growth rate factor, β_i, to the disturbance wavenumber, k, for a given fluid and sheet velocity. By differentiating β_i with respect to k and setting the resulting expression equal to zero, the wavenumber of the fastest growing disturbance, k_m, can be found. Once k_m is known, the corresponding growth rate factor can be calculated using Eq. 6.

To predict drop size characteristics, Dombrowski and Johns[14] reasoned that the sinusoidally-shaped sheet breaks into cylindrical ligaments at crest and trough points and related the ligament diameter, d_L, to the sheet thickness and wavenumber as:

$$d_L = \sqrt{\frac{4h}{k_m}} \tag{7}$$

The ligaments subsequently break up into drops as a result of surface tension induced symmetrical wave growth. Dombrowski and Johns[14] assumed that the wave grows until the disturbance amplitude is equal to the ligament radius, thus resulting in one drop per wavelength. The drop size, d_D, for water in air is then

$$d_D = \left(\frac{3\pi}{\sqrt{2}}\right)^{\frac{1}{3}} d_L\left[1+\frac{3\nu_l\rho_l}{\sqrt{\rho_l\sigma d_L}}\right]^{\frac{1}{6}} = 1.89 d_L \tag{8}$$

Taylor[7] made detailed measurements of the thickness and lateral spread of sheets formed by low-speed (<5.6 m/s) impinging water jets and noted[7,20] that the overall shape of the sheet was related to the presence of stationary antisymmetric waves within a limiting radius, which was defined as the radius where the Weber number based on local sheet thickness is unity. His measurements showed that

the sheet thickness, h, at any radial location, r, on the sheet was of the form, $rh=F(\theta,\phi)$, which is independent of U_s. Hasson and Peck[22] used Taylor's[7] data to verify their analytically derived expression for the sheet thickness,

$$h = \frac{d_j^2 \sin^3\theta}{4r(1-\cos\phi\cos\theta)^2} \tag{9}$$

where d_j is the jet diameter.

Ibrahim and Przekwas[9] extended Taylor's[19] work to obtain an analytical solution for the shape of the sheet at low Weber numbers ($We<500$), while for the high Weber number regime ($We>2000$), they suggested the use of Weihs' analysis.[15] In the low Weber number regime, the authors suggested that stationary antisymmetric waves determine the shape of the sheet, which agrees with prior studies by Taylor[19] and Huang.[6] In the low Weber number regime, the expression for the sheet shape took the following form:

$$r_b = \frac{d_j h_o}{2h_e \sin\theta} \tag{10}$$

where r_b is the distance from the impingement point to the sheet edge, and h_o and h_e are the initial and edge sheet thicknesses, respectively. Details for calculating the initial and edge sheet thicknesses can be found in Ref. 9.

The semi-empirical theoretical models discussed above predict the sheet shape for the low Weber number regime, and the sheet breakup length and drop size for the high Weber number regime. These parameters form the basis for comparisons with the experimental results obtained in the present study.

Experimental Studies of Impinging Liquid Jets

Experimental studies on impinging injector systems have mainly been concerned with developing mean drop size and mixing efficiency correlations from cold flow measurements.[23-28] and under combusting conditions.[28] Studies that shed light on the important physical mechanisms controlling sheet

breakup and subsequent drop size formation have been less numerous;[4-8] important results from these studies are summarized below.

Heidmann *et al.*[4] performed an extensive experimental study on the atomization characteristics of two turbulent impinging jets as a function of orifice diameter, d_o, length-to-diameter ratio, L/d_o, pre-impingement length, l_j, jet velocity, U_j, impingement angle, 2θ, dynamic viscosity, μ_l, and surface tension, σ. From flash photographs, Heidmann *et al.*[4] identified four spray patterns. The first spray pattern termed the *closed rim* regime was characterized by a smooth liquid sheet surrounded by a thick rim that contained the major portion of liquid. This sheet pattern occurred at velocities below 4 m/s. The next observed spray pattern was the *periodic drop* pattern in which waves were evident on the sheet surface. In addition, drops detached tangentially off the sheet periphery at periodic intervals. The velocity range for this pattern was between 4 to 9 m/s. The *open rim* pattern, also observed between jet velocities of 4 to 9 m/s, was characterized by a thinning sheet, and unlike the *closed rim* pattern, the outside rim did not meet at the spray centerline. The last spray pattern identified was the *fully developed* pattern in which waves of drops were shed in a periodic fashion from the sheet edge. *Fully developed* sprays were observed for jet velocities greater that 10 m/s. Heidmann *et al.*[4] also noted that there was a sharp transition between *open rim* and *fully developed* regimes.

In addition to identifying the four sheet patterns, Heidmann *et al.*[4] measured the shedding frequency of ligaments and drops from the edge of the sheet and found that this "wave frequency" was linearly proportional to $U_j \cos\theta$. The "wave frequency" decreased with increasing impingement angle, while remaining relatively insensitive to changes in orifice diameter and pre-impingement length. An important observation made in this study was the similarity between the measured "wave frequency" and the frequency of high-frequency instability modes observed in liquid rocket engines.[1,4]

Dombrowski and Hooper[5] performed an experimental study on turbulent and laminar impinging water jets. Dombrowski and Hooper[5] measured the sheet speed using high speed cinematography and

drop size from flash photographs as a function of jet velocity and impingement angle. Distinct sheet structure differences were seen between the laminar and turbulent impinging jet cases. The sheet formed from laminar impinging jets tended to produce much larger and smoother sheets as compared to the sheets formed by turbulent impinging jets. Measured sheet velocities tended to be between the velocity of the jet and the value of $U_j \cos\theta$.

Dombrowski and Hooper[5] suggested that sheet breakup does not scale with Reynolds number, but is dependent on the jet velocity profile and impingement angle. For turbulent jets, "impact waves" formed at the impingement point disintegrated the sheet. For the laminar impinging jets, both "impact waves" and aerodynamic waves affected the sheet disintegration process. The authors[5] also stated that the wavelength of both "impact waves" and aerodynamic waves and the breakup length decrease with increasing jet velocity. However, breakup length measurements made from their photographs dispute the latter statement.

Huang[6] experimentally and analytically studied the breakup of liquid sheets formed by two opposing water jets ($2\theta = 180°$) injected through standard ASME sharp edged orifices at jet velocities between 2 to 20 m/s. Huang[6] presented the measured nondimensional breakup radius ($r_b/0.5d_o$) versus Weber number ($\rho_l U_j^2 d_o/\sigma$), and indicated two Weber number dependent breakup regimes connected by a transition regime.

In the first regime, $100 < We < 500$, the circular sheets were stable with a nearly perfect circular edge and the nondimensionalized breakup radius increased with increasing Weber number. Huang[6] occasionally saw disturbances originating from the impingement point in this regime akin to the "impact waves" observed by Dombrowski and Hooper.[5] Huang[6] performed a force balance between the inertia and surface tension forces acting on the circular sheet to obtain an expression that related the nondimensional breakup radius to the Weber number (for $We < 900$).

The transition regime spanned a Weber number range from 500 to 2000. Huang[6] noted that cardioid waves emerged and predominated in part of this region ($500 < We < 800$). The nondimensional breakup radius reached a maximum between Weber numbers of 800 and 1000, and antisymmetric waves first appeared in this regime.

Huang[6] referred to the second breakup regime, $We > 2000$ (the maximum We for his experiments was 30000), as the unstable liquid sheet regime where "the sheet flaps with a flag-like motion." In this regime, the nondimensional breakup radius decreased with increasing Weber number. Based on an analysis for a vibrating membrane, a semi-empirical relation for the breakup radius was developed[6]

$$\frac{r_b}{\frac{1}{2}d_o} = 14.2\, s^{-\frac{2}{3}} We^{-\frac{1}{3}} \tag{11}$$

Anderson *et al.*[8] investigated the spray characteristics of turbulent impinging jets by measuring the sheet breakup length, x_b, maximum sheet width, W, and drop size as a function of flow velocity and injector geometry (2θ, d_o, L/d_o and l_j). The experimental apparatus and the operating conditions of the impinging jet system were very similar to those of Heidmann *et al.*[4] In this study, the authors[8] found the breakup length to increase with decreasing impingement angle and increasing jet velocity, up to the maximum velocity tested (18.5 m/s), which agrees with observations made in previous experimental studies.[4] The maximum sheet width, W, was relatively independent of jet velocity and impingement angle. Changes in orifice L/d_o did not appreciably affect the spray characteristics, while variation in the pre-impingement length, l_j, had a measurable effect on breakup length and drop size. Drop size and velocity measurements made with the Phase Doppler Particle Analyzer (PDPA) at the spray centerline downstream of the impingement point showed the drop size decreasing with increasing jet velocity and increasing impingement angle, and that the drop velocity was nearly equal to the jet velocity. Analysis using linear stability theory provided predictions of drop size that reproduced the experimental trends; however, breakup length predictions did not follow the experimental trends.

Experimental

The atomization characteristics of two impinging water jets were experimentally evaluated using the experimental arrangement shown in Fig. 2 which is similar to that used by Heidmann *et al.*[4] and Dombrowski and Hooper.[5] and is essentially identical to that used by Anderson *et al.*[8] The experimental setup allowed for variation of the impingement angle and size (length and diameter) of the precision bore glass tubes. Precision bore glass tubes were utilized to minimize effects of surface roughness. Minor spatial adjustments to assure precise alignment of the impinging jets were provided by a micrometer stage mounted on one of the lines. The impinging jets were deemed to be aligned correctly when the plane including the two jets was visually observed to be normal to the plane of the resulting sheet. PDPA measurements in the spray field resulted in radial profiles of drop size that were symmetric about the centerline,[8] and showed that this simple procedure yields correct alignment. The flow system consisted of a 9.47-liter (2.5-gallon) tank filled with water pressurized by compressed nitrogen gas. The flowrate was monitored using rotameters, while the pressure drop across the glass tubes was measured using pressure gauges. Both turbulent and laminar impinging jets were studied. Experimental intricacies of each case are discussed below.

Turbulent Impinging Jets

Precision bore glass tubes were attached to 4.57 mm inner diameter, I.D., (6.35 mm outer diameter, O.D.) stainless steel tubes with fittings. The diameter and length of glass tubes used for the turbulent impinging jet experiments in this study were the same as those used by Heidmann *et al.*[4] The tube orifice diameters were 0.64 mm, 1.02 mm and 1.45 mm, while the length of the tubes was 50.8 mm; thus yielding a length-to-diameter ratio of 80, 50 and 35, respectively. The inlet of the glass tubes was sharp and the ratios of fitting diameter (6.35 mm I.D.) to glass tube diameters were 9.92, 6.23 and 4.38, respectively. The pre-impingement length, l_j, for these turbulent impinging jet experiments was set to be 25.4 mm, thus yielding pre-impingement length-to-orifice diameter ratios, l_j/d_o, of 40, 25

and 18 for the three aforementioned tube geometries, respectively. Measurements were made at impingement angles, 2θ, of 40°, 60° and 80°. The velocity of the water jets ranged between 5-20 m/s. The two water jets were turbulent since for all the velocities and diameters studied, the Reynolds number was greater than 2300. In addition, no special contouring procedures were taken to ensure laminar flow and the jet surface always appeared ruffled.

Instantaneous images of the spray field were taken using diffuse backlighting provided by a strobe light with a time duration of approximately 5 μs, while a CID solid state camera (512 by 512 pixels) was used to acquire the spray images. Typically, 17 spray images were obtained for each unique geometric and operating condition. From the spray images, the breakup length, x_b, and the distance between any adjacent periodic structures, λ, were measured. The breakup length was defined as the distance from the impingement point along the spray centerline to where the intact sheet disintegrates into ligaments and drops, which is the same definition given by Heidmann *et al.*[4] From the 17 spray realizations, the average value and corresponding standard deviation of the aforementioned measured parameters was obtained. High-velocity water jets emanating from small L/d_o tubes can lead to cavitation. For the cases presented here, no cavitation effects were observed. The cavitation number, defined as the ratio of the upstream pressure less the liquid's vapor pressure to the pressure drop across the orifice, was calculated for the various measurement conditions and compared with Nurick's critical cavitation number.[29] The cavitation behavior of the jets was found to be generally consistent with the results observed by Nurick[29] and is more fully discussed in Ref. 8.

Drop size and velocity measurements were made for the 0.64 mm diameter glass tube turbulent impinging jet case using an argon-ion (λ=514.5 nm) laser-based, Fast Fourier Transform (FFT) version of the Phase Doppler Particle Analyzer (PDPA).[30,31] The theory behind the operation of the PDPA has been reviewed thoroughly in the literature.[30,31] hence only a few system details are mentioned here. The collection optics were oriented 30° off axis from the forward propagation direction of the laser beam.

which is the optimum angle for measuring transparent drops.[30] The optical configuration of the transmitting and collection optics chosen allowed the measurement drop size range to span 40 to 1400 μm.

Drop size/velocity measurements for a set of parametric conditions were made in a previous study[8] at two locations downstream of the impingement point, $x=16$ and 41 mm. At each downstream location, measurements were made at 6.4 mm increments in the plane of the sheet normal to the sheet centerline.[8] In this study, only the drop size measurements at a single spatial location ($x=16$ mm, along the sheet centerline) are presented as a function of jet velocity and impingement angle. At each measurement location, 8000 drops were measured, since at least 5500 data points are needed for $\pm$ 5% accuracy in mean diameter measurements.[32]

Laminar Impinging Jets

A series of experiments involving laminar impinging jets was also undertaken using the experimental setup shown in Fig. 2. For these tests, 0.51-mm-diameter precision bore glass tubes with an L/d_o ratio of 375 were used. The large L/d_o ratio ensures fully developed flow. These tubes are very similar to those used by Dombrowski and Hooper.[5] Each glass tube was attached to a 12.7-mm-O.D., 10.4-mm-I.D. brass tube with fittings. To ensure laminar flow through the precision bore glass tubes, an inlet glass tube was contoured such that the fluid transitioned smoothly from the brass tube to the glass tube. The transition angle between the inlet glass tube wall and the tube centerline was 17°. This contoured inlet tube was fused to the 0.51-mm-I.D. precision bore glass tube.

Contouring the inlet extended the Reynolds number range for laminar flow up to 10000 as indicated by pressure drop measurements taken across the glass tube, and the glass-like appearance of the jets. Often, a "bursting phenomenon", attributed to velocity profile relaxation effects,[33] was observed where the smooth laminar jet would suddenly and violently turn chaotic at some distance from the tube exit.

As with the turbulent impinging jets, instantaneous images of the laminar impinging jet spray were taken using the CID camera and strobe light. Approximately 17 images at each operating and geometric condition were acquired from which the breakup length was measured. An average value and standard deviation of the two measured quantities were determined, and compared to model predictions and previous experimental studies.

Results and Discussion

The disintegration of sheets formed by two impinging liquid jets is modeled using two existing theories; a stationary antisymmetric wave-based theory for low Weber numbers,[9] and a linear stability-based theory for high Weber numbers.[8] The stationary antisymmetric wave-based theory yielded the shape of the sheet from which the breakup length was obtained, while the linear stability-based theory yielded breakup length and drop size predictions. The breakup length predictions of both theories, and the drop size predictions from the linear stability-based model are compared to experimental measurements. Breakup length measurements were made for both laminar and turbulent impinging jets, while drop size measurements were made only for the turbulent impinging jet case. Finally, measurements of the distance between apparent wave-like structures on the sheet surface are presented for the turbulent impinging jet case as a function of jet velocity and orifice diameter.

General Spray Characteristics

The sheets typically produced by turbulent impinging water jets are shown in Fig. 3. Here, the orifice diameter was 0.64 mm and the jet velocities were 6.4 and 18.5 m/s. The free jet length prior to impingement, or pre-impingement length, l_j, was 25 mm, L/d_o was 80 and the impingement angle, 2θ, was 60°. The two instantaneous images shown in Fig. 3 fall into the *fully developed* regime identified by Heidmann *et al.*[4] It is interesting to note the apparent periodic nature of both the disturbances on the sheet surface and the detaching ligaments. Recall that Heidmann *et al.*[4] measured the "wave frequency" of detaching ligaments and drops and observed it to be linearly proportional to $U_j \cos\theta$.

Instantaneous images of sprays resulting from impinging laminar water jets are shown in Fig. 4. In this case, the orifice diameter was 0.51 mm, the jet velocities were 7.1 and 17.9 m/s, L/d_o was 375, the impingement angle was 60° and the pre-impingement length, l_j, was approximately 10 mm. The images in Fig. 4 have the same scale as the images for the turbulent impinging jet case shown in Fig. 3. Despite the similarity between the operating and geometric parameters of the turbulent and laminar cases, the appearance of the sheets produced in each case is quite different. The sheets resulting from the impinging laminar jets are larger than their turbulent counterparts. In addition, the sheets for the laminar case tend to be much smoother and less chaotic. Dombrowski and Hooper[5] also observed distinct differences between turbulent and laminar impinging jet cases, and attributed these differences primarily to the different velocity profiles across the jets for the two cases. Dombrowski and Hooper[5] stated that "impact waves" originating from the impingement point were responsible for sheet disintegration for the turbulent impinging jet case as well as for the breakup of sheets formed by high speed laminar impinging jets. These "impact waves" can be seen in the U_j=17.9 m/s image of Fig. 4, and appear to lead to the disintegration of the sheet. Careful inspection of the high velocity case in Fig. 4 reveals tears at the center of the intact sheet as well. In addition, the "impact waves" are dominant in the center portion of the sheet. Dombrowski and Hooper[5] stated that the slower moving fluid at the sheet periphery resulting from the laminar velocity profile across the jet tended to damp out the "impact waves".

The images presented here demonstrate the importance of the jet condition prior to impingement in understanding the atomization process. The differences between laminar and turbulent impinging jet conditions involve details related to the velocity profile and turbulence intensity of the jets prior to impingement. Despite the clear importance of the jet's initial condition on the atomization process, no definitive studies presently exist to clearly differentiate velocity profile and turbulence intensity effects on atomization. Actual impinging injectors have small L/d_o values (typically less than five) and *Re*

numbers which lie in the turbulent regime (typically 10^6). Thus, the velocity profiles developed under these short L/d_o ratios will not correspond to fully developed conditions. Furthermore, high turbulence intensity levels are to be expected in actual conditions due to the flow-turning effects encountered in the injector manifold of typical rocket engines. The degree to which such phenomena control the atomization process remains a serious challenge to experimentalists and modelers interested in impinging jet injectors.

Analysis

The linear stability-based model was used to predict breakup length and drop size. For these predictions to be made, the sheet velocity, U_s, must be known. Drop velocity measurements made in a previous study for turbulent impinging jets[8] indicated that for the entire tested velocity range (5 to 25 m/s) and impingement angle range (40°and 100°), the mean drop velocity was close to the jet velocity, U_j. This result suggests that the sheet speed is the same as the speed of the incoming jets, U_j. Taylor[7] also noted that the jet and sheet speeds should be the same. Dombrowski and Hooper[5] measured the sheet speed through high speed cinematography, and found essentially similar results for the sheet velocity. Consequently, the sheet velocity, U_s, is assumed to be the same as the jet velocity, U_j. In addition, it is assumed that the jet diameter, d_j, is the same as the orifice diameter, d_o.

The first step taken was to compare Squire's[13] analysis with Dombrowski and Johns[14] and Weihs[15] analyses of viscous sheets. Weihs,[15] after simplifying his analysis, obtained the same expression relating the growth rate factor and wavenumber as Dombrowski and Johns.[14] Squire[13] provided explicit expressions for the wavenumber, k_m, (Eq. 3) and the growth rate factor, $\beta_{i,m}$, (Eq. 4) for the most unstable wave which is assumed to control the breakup process of the liquid sheet. For the viscous sheets, the wavenumber of the most unstable wave, k_m, was found from Eq. 6, taken from Weihs' analysis.[15]

The wavenumber and growth rate factor of the fastest growing wave for both the viscous and inviscid cases were calculated and compared as a function of sheet velocity and sheet thickness for a

water sheet in still air. With increasing sheet thickness and velocity, the maximum wavenumber predicted using the inviscid analysis becomes larger than that predicted by the viscous analysis. However, for the cases studied here, Squire's[13] simple expression for the wavenumber (Eq. 3) of the most unstable wave results in less than 1% deviation from the viscous analysis results.

Furthermore, for the flow and geometric conditions of this study, the maximum growth rate factor, $\beta_{i,m}$, predicted by the inviscid[13] and viscous[14,15] analyses were also the same. However, for more viscous liquids and higher gas densities (corresponding to higher chamber pressures), the two analyses will differ. Based on these observations, Squire's simple expressions for the wavenumber (Eq. 3) and growth rate factor (Eq. 4) of the most unstable wave were used to calculate breakup length and drop size.

The sheet breakup length is linked to the sheet velocity, disturbance growth rate, sheet thinning rate and the ratio of the final to the initial disturbance amplitude. Recall that the breakup length is defined as the distance from the impingement point to where the intact sheet disintegrates along the spray centerline. The empirical relation given by Eq. 2 is used to compute the breakup length, x_b, using the maximum growth rate factor, $\beta_{i,m}$ (see Eq. 4), derived by Squire.[13] Inspection of Eq. 4 indicates the need for a sheet thickness expression. For the sheet thickness, Hasson and Peck's[22] expression (Eq. 9) was used. With the three aforementioned equations, an explicit expression for the breakup length, x_b, was derived as follows:

$$\frac{x_b}{d_o} = 5.451 s^{-\frac{2}{3}} [We f(\theta)]^{-\frac{1}{3}} \tag{12}$$

where d_o is the orifice diameter, s is the ratio of gas density to liquid density, We is the Weber number based on liquid properties, jet velocity and orifice diameter, and $f(\theta)$ is given as follows:

$$f(\theta) = \frac{(1-\cos\theta)^2}{\sin^3\theta} \tag{13}$$

where θ is the impingement half-angle. Note that the constant given by Eq. 13 is contained in the sheet thickness equation of Hasson and Peck[22] (Eq. 9) for $\phi=0°$ (spray centerline). If a different expression

for the sheet thickness was used, then $f(\theta)$ would have a different form. For conditions involving more viscous liquids and/or higher gas densities, the expression for the growth rate factor, β_i, for the viscous case given by Eq. 6, and Hasson and Peck's[22] sheet thickness relation (Eq. 9) can also be used in conjunction with the empirical breakup relation, Eq. 2. The resulting expression could then be numerically integrated as a function of wavenumber to solve for the breakup length.[8]

Sheet Breakup Length Measurements

Sheet breakup length was calculated using Eq. 12, and compared to breakup length measurements made for both laminar and turbulent impinging jets. The numerical integration procedure outlined for the viscous case was also carried out and, as expected, the breakup length was identical to that predicted by Eq. 12. The nondimensional breakup length, x_b/d_o, is plotted as a function of the nondimensional scaling parameter $We(1\text{-}\cos\theta)^2/\sin^3\theta$ in Fig. 5. For the experimental measurements, each symbol represents an average of 17 measurements, and the corresponding bars represent the $\pm$ standard deviations. The results obtained using linear stability-based theory collapse to a single line when plotted in the manner shown in Fig. 5. However, the measurements do not collapse in a similar fashion. Breakup length measurements for turbulent impinging water jets (d_o=0.64 mm, L/d_o=80) were made at discrete velocities of 6.4, 12.4 and 18.5 m/s and at impingement angles of 40°, 60° and 80°. For the laminar impinging jet case (d_o=0.51 mm, L/d_o=375), breakup length measurements were made at discrete velocities of 7.1, 13.3 and 17.9 m/s, and impingement angles of 40°, 60° and 80°. It should be noted that different precision bore glass tubes used for the laminar cases sometimes led to different breakup length results. This measurement variability was likely due to small differences in tube inlets (i.e., transition angle), tube outlets and internal surface conditions. The measurements were duplicated with several sets of glass tubes. The sensitivity of the sheet breakup process to apparently small variations in the tube characteristics for the laminar case reinforce the observation that the jet conditions strongly affect the spray formation process.

The predicted nondimensional breakup length decreases with an increase in the scaling parameter. However, the opposite trend is observed for the turbulent case measurements for all impingement angles. For the laminar impinging case, the nondimensional breakup length increases to a maximum, then decreases with increasing Weber number. The linear stability-based model also overpredicts the magnitude of the breakup length. However, the predicted breakup length magnitude can be altered by choosing a constant different than the one in Eq. 2.

Several conclusions can be drawn by comparing the laminar and turbulent impinging jet cases to each other as well as with the results of previous studies. For the turbulent impinging jet case, the breakup length decreases with increasing impingement angle, which is opposite to the general trend observed for the laminar jet case. Intuitively, the breakup length would be expected to increase with decreasing impingement angle since an increasing amount of momentum is directed in the axial direction and the sheet is thicker on the centerline. Dombrowski and Hooper[5] indicated that "impact waves" controlled the breakup of sheets formed by impinging turbulent jets, and that the breakup length would decrease with increasing jet velocity; this trend is not observed for the cases studied here. The opposing trend of breakup length as a function of impingement angle for the laminar and turbulent cases suggests that different breakup mechanisms are operative.

As mentioned previously, the breakup length increases to a maximum, then decreases for increasing Weber number for the laminar impinging jet case. Measurements showed that the largest breakup length typically occurred between Weber numbers of 550-725. Huang,[6] in his study of opposed impinging jets ($2\theta = 180°$), showed that the breakup radius (or length) increased linearly to a maximum value and then decreased with increasing Weber number. The breakup radius reached a maximum between Weber numbers of 800 to 1000. For Huang's case of $2\theta = 180°$, the trigonometric term in the nondimensional scaling parameter, $(1-\cos\theta)^2/\sin^3\theta$, is one; therefore, his data for breakup radius increases linearly for the entire range of the abscissa shown in Fig. 5. However, direct comparisons between his

results and the current data is clouded by the different jet conditions of the two sets of experiments. Huang[6] used sharp-edged ASME orifices, which indicates that the jet velocity profile was "plug flow" and probably had low turbulence intensity levels. Also, the equation derived by Huang[6] for breakup radius (Eq. 11) ($We > 1000$) is similar to the equation derived here (Eq. 12). Inspection of the two equations shows that other than the constants, the exponents of both the We and s terms are identical. The constants differ because Huang[6] obtained the value for his constant by curve-fitting the equation to the data.

Dombrowski and Hooper[5] suggested that "impact waves" were responsible for sheet breakup for intermediate to high speed laminar impinging jets, and for all but the lowest velocities for turbulent impinging jets. This idea seems plausible since the breakup length for both the laminar and turbulent impinging jet cases approach similar values at high jet velocities (see Fig. 5). In addition, flash photographs of the sheets under the previously mentioned conditions indicate the presence of disturbances which appear to originate at the impingement point.

Ibrahim and Przekwas[9] proposed that their extension of Taylor's[19] stationary antisymmetric wave-based theory should be used in a low Weber number regime ($We < 500$), while linear stability theory should be applied to a high Weber number regime ($We > 2000$). In the low Weber number regime, the shape of the sheet is predicted using Eq. 10. The sheet shape predicted using the aforementioned equation is shown in Fig. 6 as a function of the impingement angle for an orifice diameter of 0.51 mm and a jet velocity of 7.1 m/s. Note that the impingement point is at x=0, y=0. The predicted sheet shape for $2\theta = 60°$ looks similar to the corresponding image for the same conditions shown in Fig. 4 (low jet velocity case, $U_j = 7.1$ m/s). From the shape of the sheet, the breakup length, x_b, can be obtained. The predicted sheet shapes have pointed tips, except for the opposed jet case ($2\theta = 180°$). For the laminar impinging jet case (experimental), sheets with pointed tips were observed for all impingement angles

tested up to a Weber number of about 350. For Weber numbers greater than 350, the sheets disintegrated before a pointed tip was formed.

Further perusal of Fig. 6 indicates that the breakup length increases with increasing impingement angle up to about 100°, after which it decreases. However, the maximum sheet width increases with increasing impingement angle up to a maximum at $2\theta=180°$. For the impingement angles studied in the present experiments ($2\theta=40°$, 60° and 80°) for the laminar impinging jet case, the general trend was for increasing breakup length with increasing impingement angle, the same trend predicted by the model. Since breakup length measurements were not made for impingement angles greater than 100°, the decrease in breakup length with increasing impingement angle for impingement angles greater than 100° as predicted by the model cannot be either confirmed or contradicted.

A comparison between the breakup length predicted by linear stability-based theory, Ibrahim and Przekwas'[9] extension of Taylor's[19] stationary antisymmetric wave theory, and the breakup length measurements for the laminar and turbulent cases is shown in Fig. 7. Specifically, the nondimensional breakup length, x_b/d_o, is plotted as a function of the non-dimensional scaling parameter, $We(1-\cos\theta)^2/\sin^3\theta$, for an impingement angle of 60°. As seen in Fig. 7, the breakup length as predicted by the Ibrahim and Przekwas[9] model is linearly proportional to Weber number, whereas for the linear stability-based model, it is proportional to $We^{-1/3}$. The breakup length predictions from the Ibrahim and Przekwas[9] model overpredict the breakup length measurements made for both the laminar and turbulent cases; however, the measured breakup length does increase with increasing Weber number, but not as strongly as the stationary antisymmetric wave-based model predicts. The model also predicts sheet shapes with pointed tips, as shown in Fig. 6. These sheets were only observed in the laminar impinging jet case for Weber numbers less than 350, which correspond to the first two data points for the laminar case in Fig. 7. As mentioned previously, the sheets formed by laminar impinging jets disintegrated before pointed tips were formed for Weber numbers greater than 350, thus explaining why longer sheets are predicted using

the stationary antisymmetric wave-based model. For the turbulent impinging jet case, the measured nondimensional breakup lengths for various jet diameters lie on nearly a single curve for this fixed impingement angle. The same trend is observed at the other impingement angles although different curves were observed for each angle. It should be noted that this collapse of the turbulent impinging jet results to a single curve for a fixed impingement angle is a reflection of the *We* number dependence since the geometric factor in the nondimensional scaling factor remains constant for fixed impingement angle. Similar to Huang's[6] breakup radius results for opposed jets, and the present results for laminar impinging jets, it is likely that the breakup length for the turbulent impinging jet case will peak for some Weber number and then decrease.

Drop-Size Measurements

Drop-size measurements using the Phase Doppler Particle Analyzer (PDPA) for the turbulent impinging jet cases were compared to predictions of the linear stability-based model. There are two models for calculating the drop diameter. The model proposed by Dombrowski and Johns[14] (Eqs. 7 and 8) can be combined with Squire's[13] expression for the fastest growing wavenumber (Eq. 3) and the nondimensional breakup length expression derived earlier (Eq. 12), and recast in the following form:

$$\frac{d_D}{d_o} = \frac{2.62}{(12)^{\frac{1}{3}}} s^{-\frac{1}{6}} [We f(\theta)]^{-\frac{1}{3}} \tag{14}$$

where d_D is the drop diameter and $f(\theta)$ is given by Eq. 13. The relationship shows that the ratio of the drop diameter to the orifice diameter has a weak inverse dependence on the scaling parameter, $We f(\theta)$. The second model, proposed by Ibrahim and Przekwas,[9] relates the drop size to the maximum wavenumber, k_m, as

$$d_D = \frac{\pi}{k_m} \tag{15}$$

which can be recast as follows:

$$\frac{d_D}{d_o} = \frac{2\pi\sigma}{d_o \rho_g U_j^2} = \frac{2\pi}{s\,We} \tag{16}$$

By contrasting the two relationships for the nondimensional drop diameter, it is evident that the former model shows a dependence on the impingement angle, whereas the latter model is independent of the impingement angle and inversely proportional to the *We* number.

The drop size measurements are compared with the linear stability-based model predictions (Eq. 14) in Fig. 8. The drop size measurements shown in the figure are for a spatial location, $x = 16$ mm, along the sheet centerline. The abscissa in this figure is the nondimensional scaling parameter, $We\,f(\theta)$, whereas the ordinate is the drop diameter nondimensionalized with the orifice diameter. Note that the measured drop sizes are polydispersed, and the arithmetic mean diameter, d_{10}, is taken for comparison purposes. The theory predicts a monodispersed drop size distribution. The comparison shows that the drop size dependence on both the Weber number and the impingement angle is similar for both measurements and predictions. The nondimensionalization also brings the data for various impingement angles close to a single curve. It is not surprising that the measurements and theory do not match quantitatively; better agreement would be observed if a higher-order moment diameter, say a d_{30}, for the measurements were used. Alternately, a larger empirical breakup constant (currently, $\int \beta_{i,m} dt = 12$) would bring the measurements and the model predictions closer. In this vein, an empirical breakup constant, $\int \beta_{i,m} dt = 64$, yields a semi-empirical model of the form:

$$\frac{d_D}{d_o} = \frac{2.62}{(64)^{\frac{1}{3}}} s^{-\frac{1}{6}} [We\,f(\theta)]^{-\frac{1}{3}} \tag{17}$$

that represents a least-squares fit to the measured d_{10}, as shown in Fig. 8. Finally, the use of the second drop-size model (Eq. 16) predicts drop sizes which are an order of magnitude greater than those measured. Therefore, based on these observations, the former model for drop size has more merit.

Surface Wave Measurements

Heidmann *et al.*[4] measured the "wave frequency" of detaching ligaments and drops from the edge of the intact sheets formed by impinging jets as a function of operating and injector parameters. Two important results of their study[4] were that the "wave frequency" was linearly proportional to $U_j \cos\theta$, and the measured "wave frequency" closely matched the frequencies associated with observed combustion instability phenomena.

Because of the interesting results and the potential implications of the Heidmann *et al.*[4] study, similar measurements were made in this study. Specifically, for the turbulent impinging jet case, the distance between apparent adjacent periodic structures on and beyond the intact sheet surface were measured as a function of flow and injector characteristics. The types of periodic structures measured include surface waves, edge ligaments and detached ligaments, all of which are shown in Fig. 9.

The surface wave category included disturbances on the intact sheet surface. Typically, the distance between adjacent surface waves, λ_{sw}, increased with increasing distance from the impingement point. Separation distance measurements were made over the entire intact sheet whenever possible to obtain an average λ_{sw}. The separation distance of adjacent surface waves is plotted as a function of jet velocity and orifice diameter for an impingement angle of 60° in Fig. 10. Each point plotted represents an average between 10 and 50 separate measurements, depending on operating conditions, while the corresponding bars represent the $\pm$ standard deviation. Despite the large standard deviation, there is a distinct increase in λ_{sw} with increasing orifice diameter. However, for the cases studied, the separation distance was relatively insensitive to changes in jet velocity. Although not presented in graphical format, it was also found that the separation distance, λ_{sw}, was insensitive to changes in impingement angle.

Similar measurements were made for the edge and detached ligament categories. Edge ligaments were defined as strands of liquid attached to the intact sheet periphery. Detached ligaments were strands of fluid either completely or nearly completely separated from the downstream edge of the intact sheet.

In general, the average separation distance between adjacent detached ligaments was larger than that of the edge ligaments. Likewise, the average separation distance between adjacent edge ligaments was larger than that of the surface waves. Again, the trends observed for λ_{sw} were also observed for the edge ligament category. The behavior of the separation distance between adjacent detached ligaments was not as apparent as the other two categories since not enough measurements were made to yield a meaningful average and standard deviation. It is interesting to note that the measured separation distances of the surface waves and edge ligaments are similar in magnitude to the fastest growing wavelength predicted by Squire[13]

$$\lambda_m = \frac{4\pi\sigma}{\rho_g U_s^2} \tag{18}$$

However, the wavelength of the most unstable wave predicted by Eq. 18 is strongly dependent on sheet velocity and independent of the orifice diameter. This is contrary to the observed behavior of the various measured separation distances.

Summary and Conclusions

A systematic study of the atomization of impinging liquid jets investigating the effects of jet conditions (laminar versus turbulent), orifice diameter, impingement angle and jet velocity has been conducted. Results of the present study have been compared to current theories in terms of sheet breakup length, drop size and sheet shape. Experiments contrasting laminar and turbulent jet conditions clearly demonstrate that the jet conditions have a dramatic effect on the atomization process. Specifically, the measured breakup lengths for the laminar impinging jet case are longer and displayed different trends as a function of jet velocity and impingement angle than those of the turbulent impinging jet case. The present results are in complete agreement with earlier studies by Dombrowski and Hooper[5] with regards to the effects of jet conditions on impinging jet atomization. These results encourage speculation that velocity profile and turbulence characteristics of the jets strongly affect the atomization processes for

impinging jet injectors. However, quantitative assessment of the specific mechanisms controlling atomization remain to be established.

For low Weber number ($We < 350$) laminar impinging jet conditions, predictions based on stationary antisymmetric wave-based theory were within 50% of the observed breakup length. Comparisons were also made with a linear stability-based theory. The linear stability-based theory predicted a monotonically decreasing sheet breakup length with increasing Weber number which is opposite to the trend observed for turbulent impinging jets. In fact, experimental observations for both the laminar and turbulent jets argue strongly for the "impact wave" theory put forward by Dombrowski and Hooper[5] as the operative mechanism leading to sheet breakup. Thus, the current use of linear stability-based theories for describing sheet breakup for impinging jet conditions appears to be questionable for the range of conditions investigated in this study. In contrast, the linear stability-based theory provided reasonable predictive capability for drop size with respect to the trends observed for increasing Weber number and impingement angle. Measurements regarding the surface wave and periodic ligament formation for the turbulent jet studies indicate that the observed wavelengths are directly proportional to the orifice diameter and independent of jet velocity and impingement angle.

Based on the results of the present study, approaches to modeling impinging jet atomization should focus on including the "impact wave" process identified by Dombrowski and Hooper[5], which none of the current models treat. Periodic perturbations associated with the jet inertia at the impingement region are often argued to be the likely mechanism for generating "impact waves". A fundamental mechanistic model for the generation and growth of "impact waves" and their association with the subsequent atomization process is currently lacking. Additionally, the relationship between the periodic surface wave and ligament structures observed in the present work needs to be considered in light of their potential to initiate and sustain combustion instability phenomena associated with impinging jet rocket injectors.

Acknowledgements

The authors would like to thank Mr. David Grupp and Ms. Gayle Ramdeen for their assistance in carrying out the laminar impinging jet studies, and Mr. Doug Smith for his assistance in fabricating the glass tubes used in the laminar impinging jet experiments. The authors would also like to acknowledge the support of the Air Force Office of Scientific Research, Air Force Systems Command, USAF under grant number AFOSR 91-0336 as well as the support of the Penn State NASA Propulsion Engineering Research Center under grant NAGW 1356. The U.S. Government is authorized to reproduce and distribute reprints for government purposes notwithstanding any copyright notation thereon.

References

[1]Anderson, W. E., Ryan, H. M. and Santoro, R. J., "Combustion Instability Phenomena of Importance to Liquid Bi-Propellant Rocket Engines," 28th JANNAF Combustion Meeting, San Antonio, TX, Oct. 28-Nov. 1, 1991.

[2]Claflin, S. E. and Volkman, J. C., "Oxygen/Hydrogen Micro-Orifice Impinging Injector Development for Modular Test Chambers," Propulsion Engineering Research Center Fourth Annual Symposium, Huntsville, AL, Sept. 9-10, 1992, pp. 53-58.

[3]*Liquid Propellant Rocket Instability*, D. T. Harrje and F. H. Reardon (eds.), NASA SP-194, 1972.

[4]Heidmann, M. F., Priem, R. J. and Humphrey, J. C., "A Study of Sprays Formed by Two Impinging Jets," NACA Technical Note 3835, March 1957.

[5]Dombrowski, N. and Hooper, P. C., "A Study of the Sprays Formed by Impinging Jets in Laminar and Turbulent Flow," *Journal of Fluid Mechanics*, Vol. 18, Part 3, 1963, pp. 392-400.

[6]Huang, J. C. P., "The Breakup of Axisymmetric Liquid Sheets," *Journal of Fluid Mechanics*, Vol. 43, Part 2, 1970, pp. 305-319.

[7]Taylor, G. I., "Formation of Thin Flat Sheets of Water," *Proceedings of the Royal Society A*, 259, 1960, pp. 1-17.

[8]Anderson, W. E., Ryan, H. M., Pal, S. and Santoro, R. J., "Fundamental Studies of Impinging Liquid Jets," AIAA Paper 92-0458, 30th Aerospace Sciences Meeting, Reno, NV, Jan. 6-9, 1992.

[9]Ibrahim, E. A. and Przekwas, A. J., "Impinging Jets Atomization," *Physics of Fluids A*, Vol. 3, No. 12, Dec. 1991.

[10]Childs, R. E. and Mansour, N. N., "Simulation of Fundamental Atomization Mechanisms in Fuel Sprays," *Journal of Propulsion*, Vol. 5, No. 6, Nov.-Dec. 1989, pp. 641-649.

[11]Rangel, R. H. and Sirignano, W. A., "Nonlinear Growth of Kelvin-Helmholtz Instability: Effect of Surface Tension and Density Ratio," *Physics of Fluids*, Vol. 31, No. 7, 1988, pp. 1845-1855.

[12]Rangel, R. and Hess, C., "Nonlinear Spacial Instability of a Fluid Sheet," AIAA Paper 90-0118, 28th Aerospace Sciences Meeting, Reno, NV, Jan. 8-11, 1990.

[13]Squire, H. B., "Investigation of the Instability of a Moving Liquid Film," *British Journal of Applied Physics*, Vol. 4, 1953, pp. 167-169.

[14]Dombrowski, N. and Johns, W. R., "The Aerodynamic Instability and Disintegration of Viscous Liquid Sheets," *Chemical Engineering Science*, Vol. 18, 1963, pp. 203-214.

[15]Weihs, D., "Stability of Thin, Radially Moving Liquid Sheets," *Journal of Fluid Mechanics*, Vol. 87, Part 2, 1978, pp. 289-298.

[16]Levich, V. G., *Physicochemical Hydrodynamics*, Prentice-Hall, Englewood Cliffs, NJ, 1962, Chapter 11.

[17]Li, X. and Tankin, R. S., "On the Temporal Instability of a Two-Dimensional Viscous Liquid Sheet," *Journal of Fluid Mechanics*, Vol. 226, pp. 425-443, 1991.

[18]Lin, S. P., Lian, Z. W. and Creighton, B. J., "Absolute and Convective Instability of a Liquid Sheet," *Journal of Fluid Mechanics*, Vol. 220, pp. 673-689, 1990.

[19]Taylor, G. I., "The Dynamics of Thin Sheets of Fluid II. Waves on Fluid Sheets," *Proceedings of the Royal Society A*, 253, 1959, pp. 296-312.

[20]Taylor, G. I., "The Dynamics of Thin Sheets of Fluid III. Disintegration of Fluid Sheets," *Proceedings of the Royal Society A*, 253, 1959, pp. 313-321.

[21]Brodkey, R. S., *Phenomena of Fluid Motions*, Addison-Wesley Series in Chemical Engineering, 1967.

[22]Hasson, D. and Peck, R. E., "Thickness Distribution in a Sheet Formed by Impinging Jets," *AIChE Journal*, Sept. 1964, pp. 752-754.

[23]Ferrenberg, A., Hunt, K. and Duesberg, J., "Atomization and Mixing Study," Contract NAS8-34504, 1985.

[24]Rupe, J. H., "Experimental Studies of the Hydrodynamics of Liquid Propellant Injection," JPL External Publication 388, 1957.

[25]Vassallo, P., Ashgriz, N. and Boorady, F. A., "Effect of Flow Rate on the Spray Characteristics of Impinging Water Jets," *Journal of Propulsion and Power*, Vol. 8, No. 5, Sept.-Oct. 1992, pp. 980-986.

[26]Hautman, D. J., "Spray Characterization of Like-On-Like Doublet Impinging Rocket Injectors," AIAA Paper 91-0687, 29th Aerospace Sciences Meeting, Reno, NV, Jan. 7-10, 1991.

[27]Knight, R. M. and Nurick, W. H., "Interim Report, Correlation of Spray Drop Size Distribution and Injector Variables," NASA Contract Report NAS7-726, Sept. 1969.

[28]George, D. J., "Rocket Injector Hot Firing and Cold Flow Spray Fields," AIAA Paper 73-1192, AIAA/SAE 9th Propulsion Conference, Las Vegas, NV, Nov. 5-7, 1973.

[29]Nurick, W. H., "Orifice Cavitation and Its Effects on Spray Mixing," *Journal of Fluids Engineering*, Dec. 1976, pp. 681-687.

[30]Bachalo, W. D. and Houser, M. J., "Phase/Doppler Spray Analyzer for Simultaneous Measurement of Drop Size and Velocity Distributions," *Optical Engineering*, Vol. 23, 1984, pp. 583-590.

[31]Ibrahim, K. M., Werthimer, G. D. and Bachalo, W. D., "Signal Processing Considerations for Laser Doppler and Phase Doppler Applications," The Fifth International Symposium on the Application of Laser Techniques of Fluid Mechanics, Lisbon, Portugal, July 9-12, 1990.

[32]Lefebvre, A. H., *Atomization and Sprays*, Hemisphere Publishing Corporation, Philadelphia, PA, 1989, p. 370.

[33]*Ibid.*, pp. 45-48.

Figure Captions

Fig. 1. Schematic diagram of a typical impinging jet spray.

Fig. 2. Schematic diagram of experimental arrangement, a) top view; b) side view.

Fig. 3. Instantaneous images of sprays formed by two turbulent impinging water jets. The jets issued from 0.64 mm inner diameter, $L/d_o=80$ precision bore glass tubes. The impingement angle, 2θ, was 60°, while the pre-impingement length, l_j, was 25 mm. Flow is from left to right.

Fig. 4. Instantaneous images of sprays formed by two laminar impinging water jets. The jets emanated from 0.51 mm inner diameter, $L/d_o=375$ precision bore glass tubes. The impingement angle, 2θ, was 60°, while the pre-impingement length, l_j, was approximately 10 mm. Note that the scale of these images is the same as those in Fig. 3. In addition, the orifice diameter and jet velocities are similar for the images in both Fig. 3 and this figure. Flow is from left to right.

Fig. 5. Nondimensional breakup length, x_b/d_o, plotted as a function of the scaling parameter $We(1-\cos\theta)^2/\sin^3\theta$, where We is the Weber number and θ is the impingement half-angle. The solid line represents predictions made using linear stability-based theory. The solid symbols represent the turbulent impinging jet case measurements ($d_o=0.64$ mm), while the hollow symbols represent the laminar impinging jet case measurements ($d_o=0.51$ mm). Each point plotted represents the mean value of 17 separate measurements, and the bars indicate the $\pm$ standard deviation of the measurements for each measurement condition.

Fig. 6. Sheet shape predictions for water in air from the Ibrahim and Przekwas[9] model plotted as a function of impingement angle. The orifice diameter was 0.51 mm, and the jet velocity was 7.1 m/s. The predicted sheet shape for the 60° impingement angle case should be compared to the corresponding spray image (Fig. 4a). Note that the scales are different.

Fig. 7. Nondimensional breakup length, x_b/d_o, plotted as a function of the scaling parameter $We(1-\cos\theta)^2/\sin^3\theta$, where *We* is the Weber number and θ is the impingement half-angle. The solid line represents predictions made using linear stability-based theory. The broken line represents breakup length predictions made using the stationary antisymmetric wave-based model for an impingement angle of 60°. The solid symbols represent the turbulent impinging jet case measurements, while the hollow symbols represent the laminar impinging jet case measurements. The experimental measurements shown are for an impingement angle, 2θ, of 60°. Each point plotted represents the mean value of 17 separate measurements, and the bars indicate the $\pm$ standard deviation of the measurements for each measurement condition.

Fig. 8. Nondimensional drop size, d_D/d_o, plotted as a function of a nondimensional scaling factor and impingement angle. Drop size predictions made using linear stability-based theory and drop size measurements made using the PDPA at an axial location of $x=16$ mm, along the spray centerline ($y=0$), are shown.

Fig. 9. A typical spray formed by two turbulent impinging water jets issuing from 0.64 mm diameter, $L/d_o=80$ glass tubes. The impingement angle was 60° and the pre-impingement length was 25 mm. Flow is from left to right. The distance between adjacent surface waves, edge ligaments and detached ligaments were measured from such spray images.

Fig. 10. The measured separation distance between adjacent surface waves, λ_{sw}, plotted as a function of jet velocity and orifice diameter for the turbulent impinging jet case at an impingement angle of 60°. Each point plotted represents an average between 10 to 50 separate measurements, while the corresponding bars indicate the associated standard deviation.

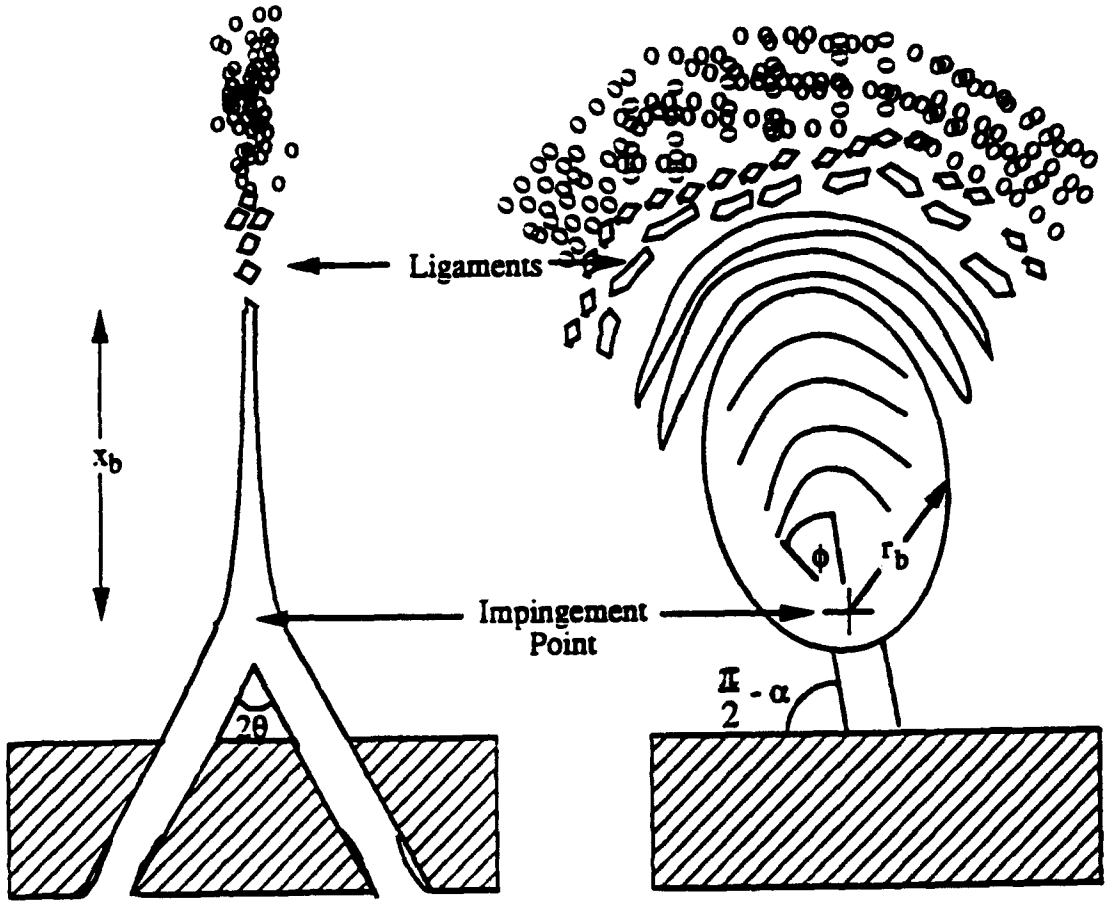
Ligaments
x_b
r_b
ϕ
Impingement
Point
2θ
$\frac{\pi}{2} - \alpha$

Fig.1

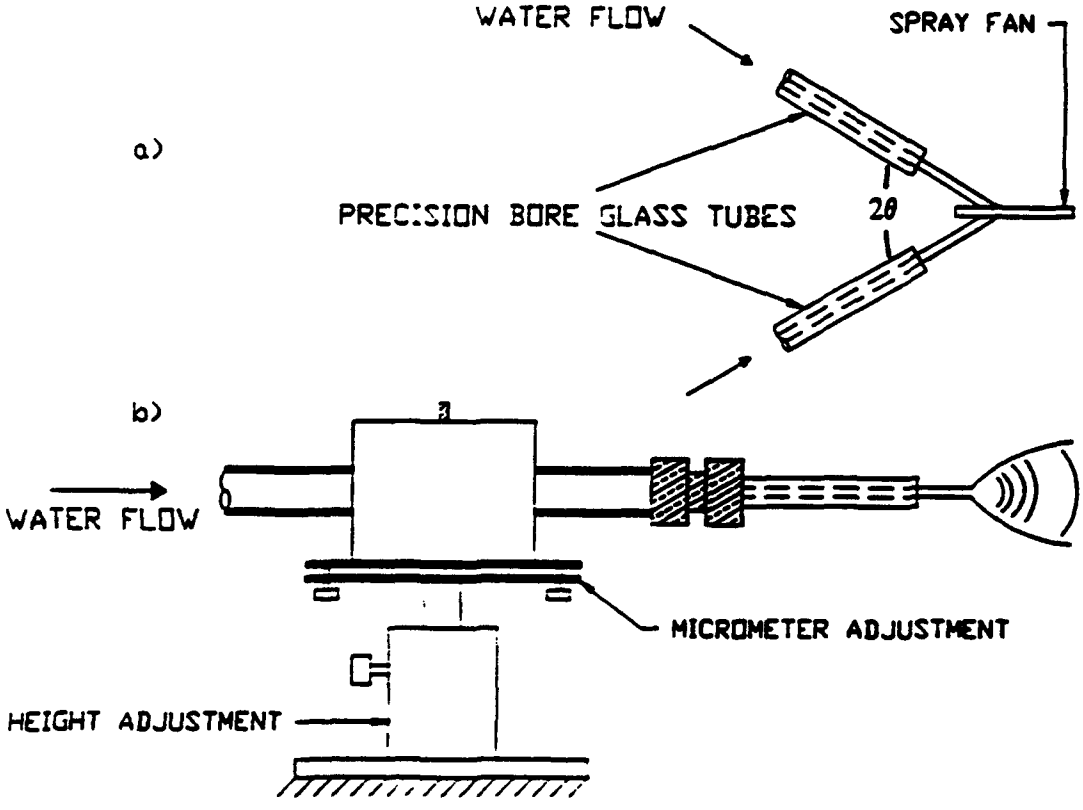
WATER FLOW
SPRAY FAN
a)
PRECISION BORE GLASS TUBES
2θ
b)
WATER FLOW
MICROMETER ADJUSTMENT
HEIGHT ADJUSTMENT

Fig. 2

3a) U_j=6.4 m/s

3b) U_j=18.5 m/s

Fig.3

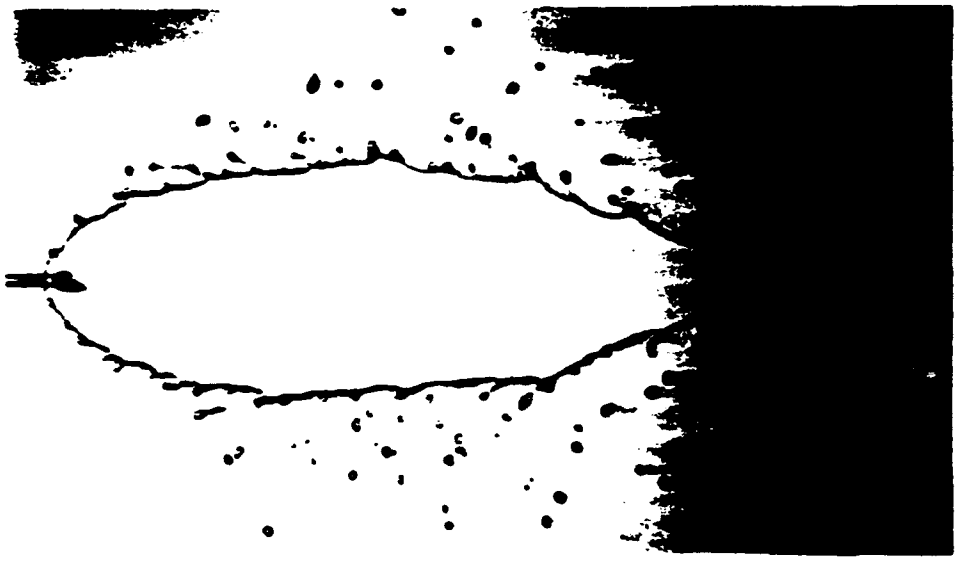

10 mm

4a) $U_\infty = 7.1$ m/s

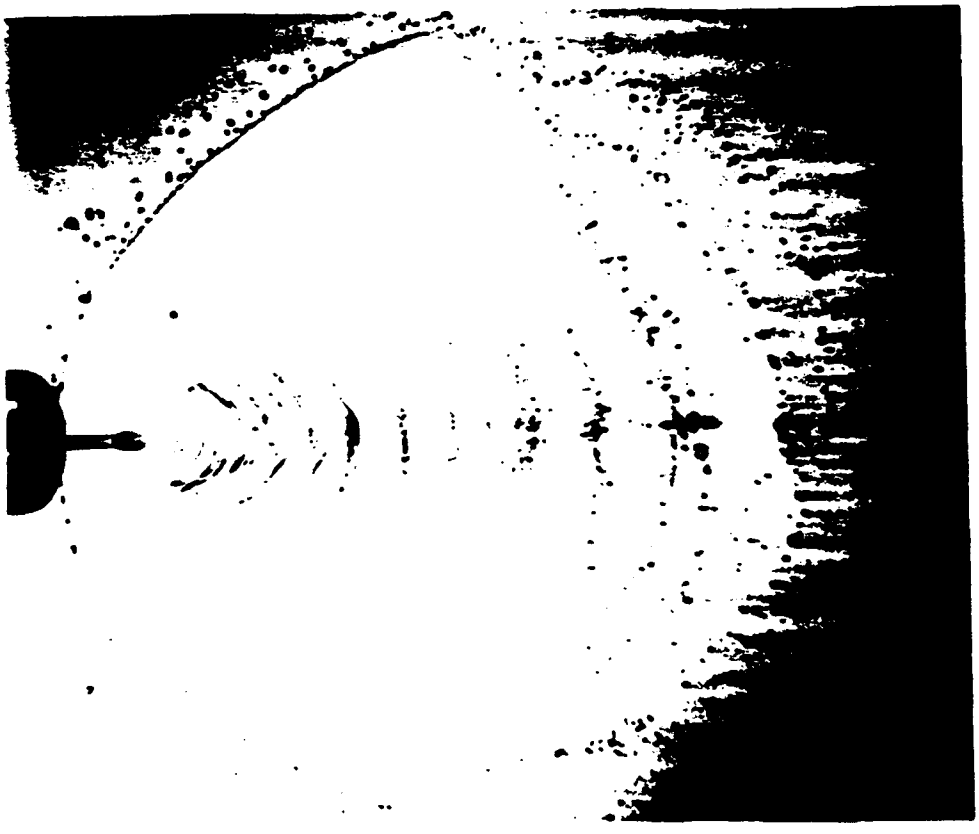

4b) $U_\infty = 17.9$ m/s

Fig. 4

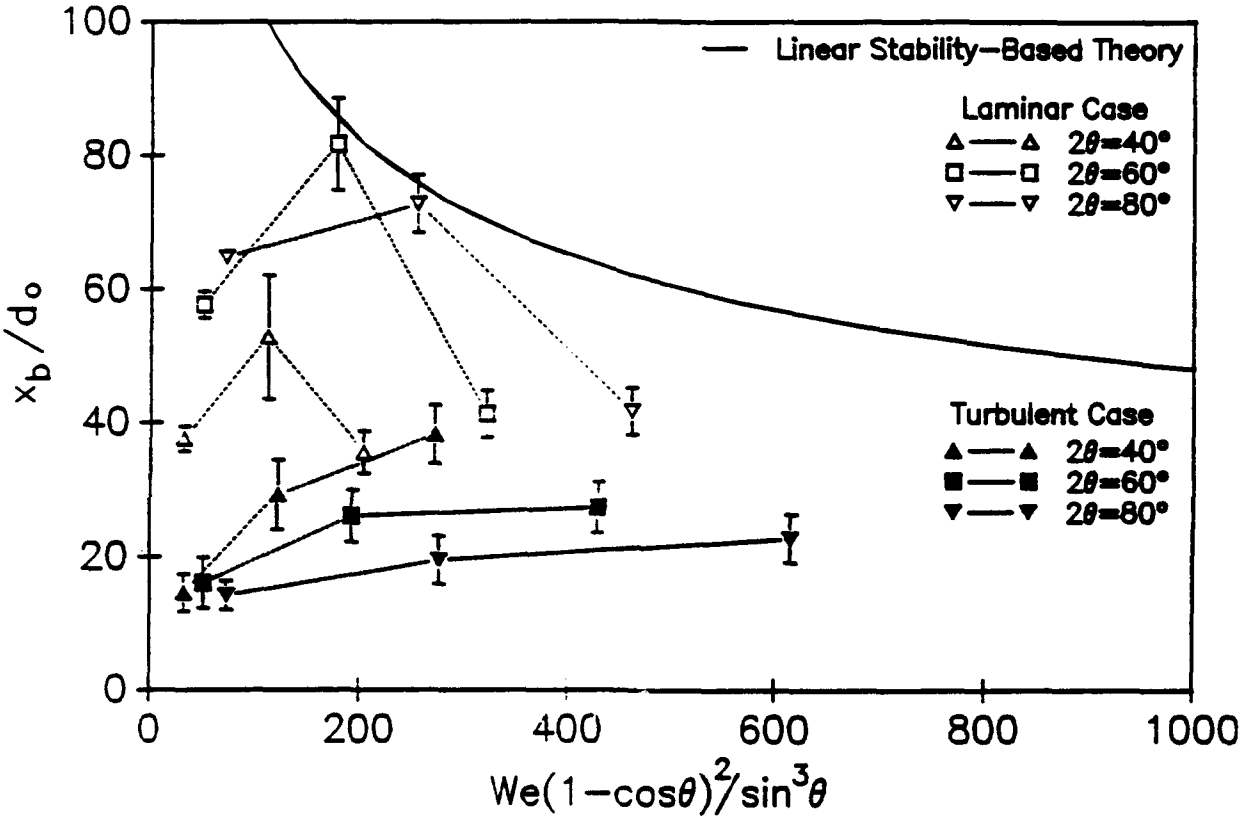
100
80
60
40
20
0
0
200
400
600
800
1000
x_b/d_o
$We(1-\cos\theta)^2/\sin^3\theta$
Linear Stability–Based Theory
Laminar Case
2θ=40°
2θ=60°
2θ=80°
Turbulent Case
2θ=40°
2θ=60°
2θ=80°

Fig 5

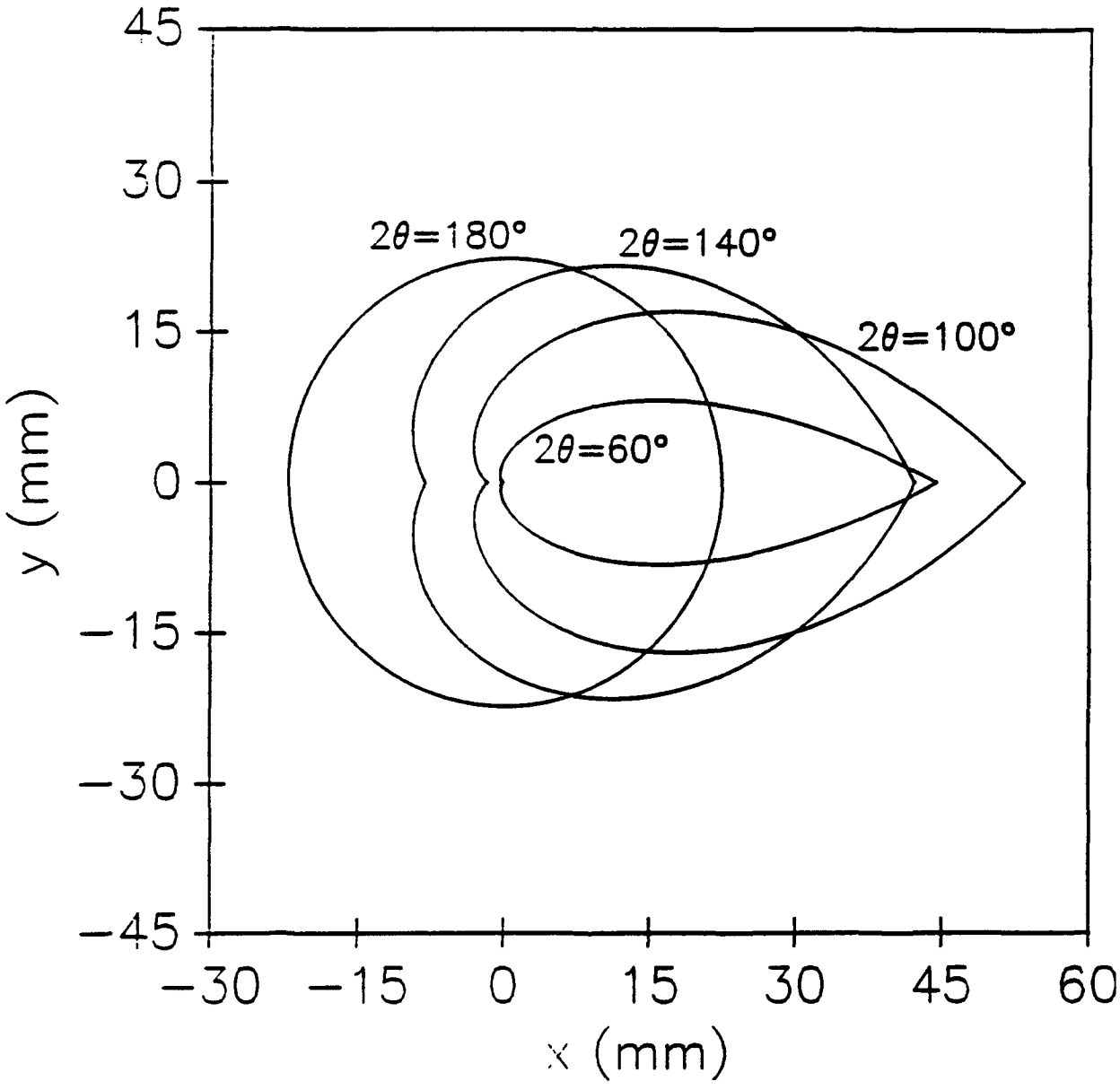
45
30
15
0
−15
−30
−45
y (mm)
2θ=180°
2θ=140°
2θ=100°
2θ=60°
−30
−15
0
15
30
45
60
x (mm)

Fig 6

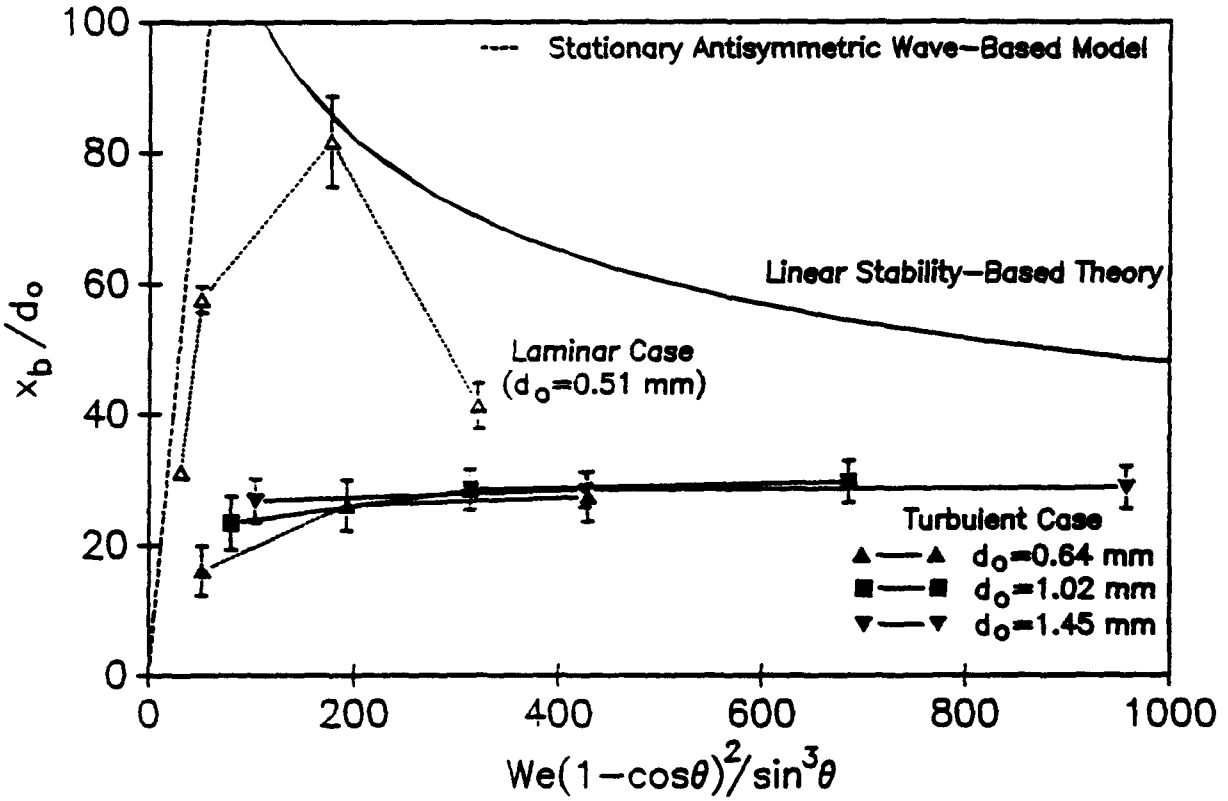
100
80
60
40
20
0
x_b/d_o
0
200
400
600
800
1000
$We(1-\cos\theta)^2/\sin^3\theta$
---- Stationary Antisymmetric Wave-Based Model
Linear Stability-Based Theory
Laminar Case
(d_o=0.51 mm)
Turbulent Case
d_o=0.64 mm
d_o=1.02 mm
d_o=1.45 mm

Fig. 7

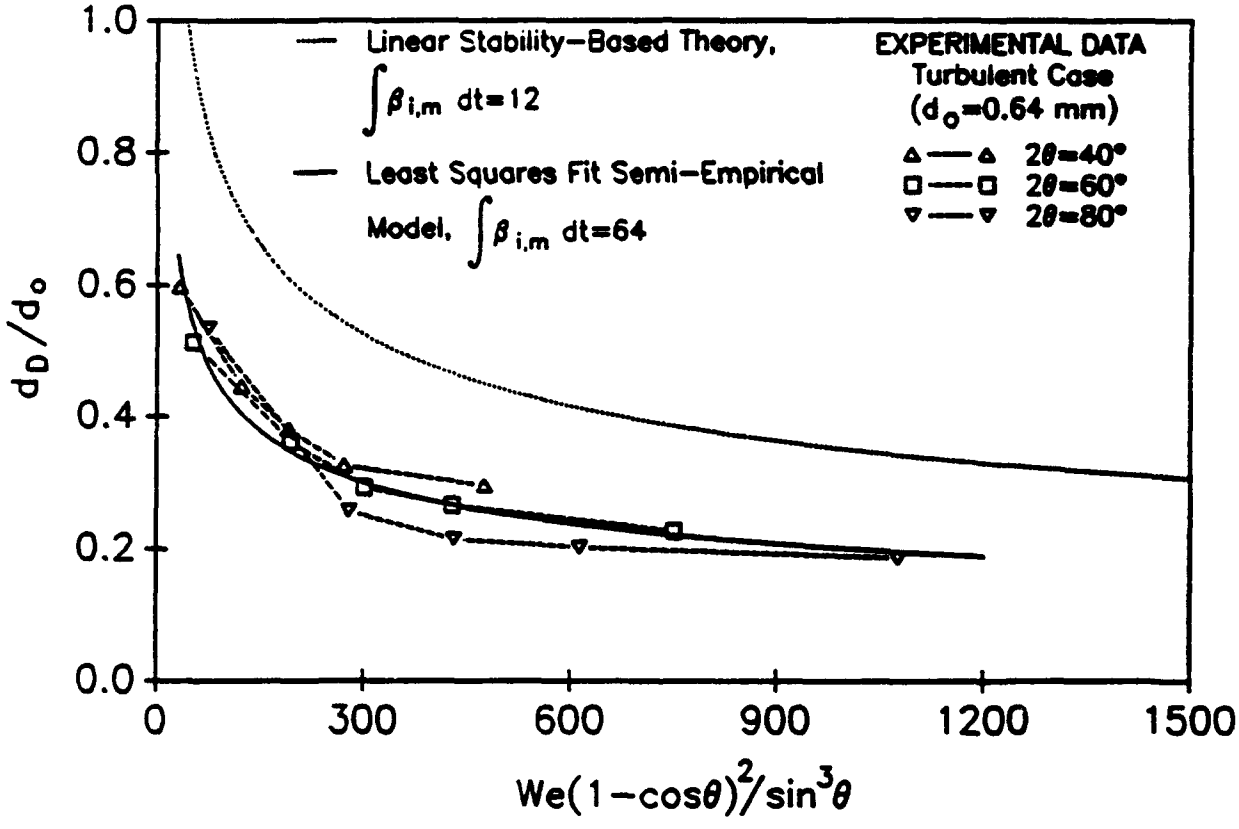
Linear Stability–Based Theory, $\int \beta_{i,m}\, dt = 12$
Least Squares Fit Semi–Empirical Model, $\int \beta_{i,m}\, dt = 64$
EXPERIMENTAL DATA
Turbulent Case
(d_o=0.64 mm)
2θ=40°
2θ=60°
2θ=80°
d_D/d_o
1.0
0.8
0.6
0.4
0.2
0.0
0
300
600
900
1200
1500
$We(1-\cos\theta)^2/\sin^3\theta$

Fig 8

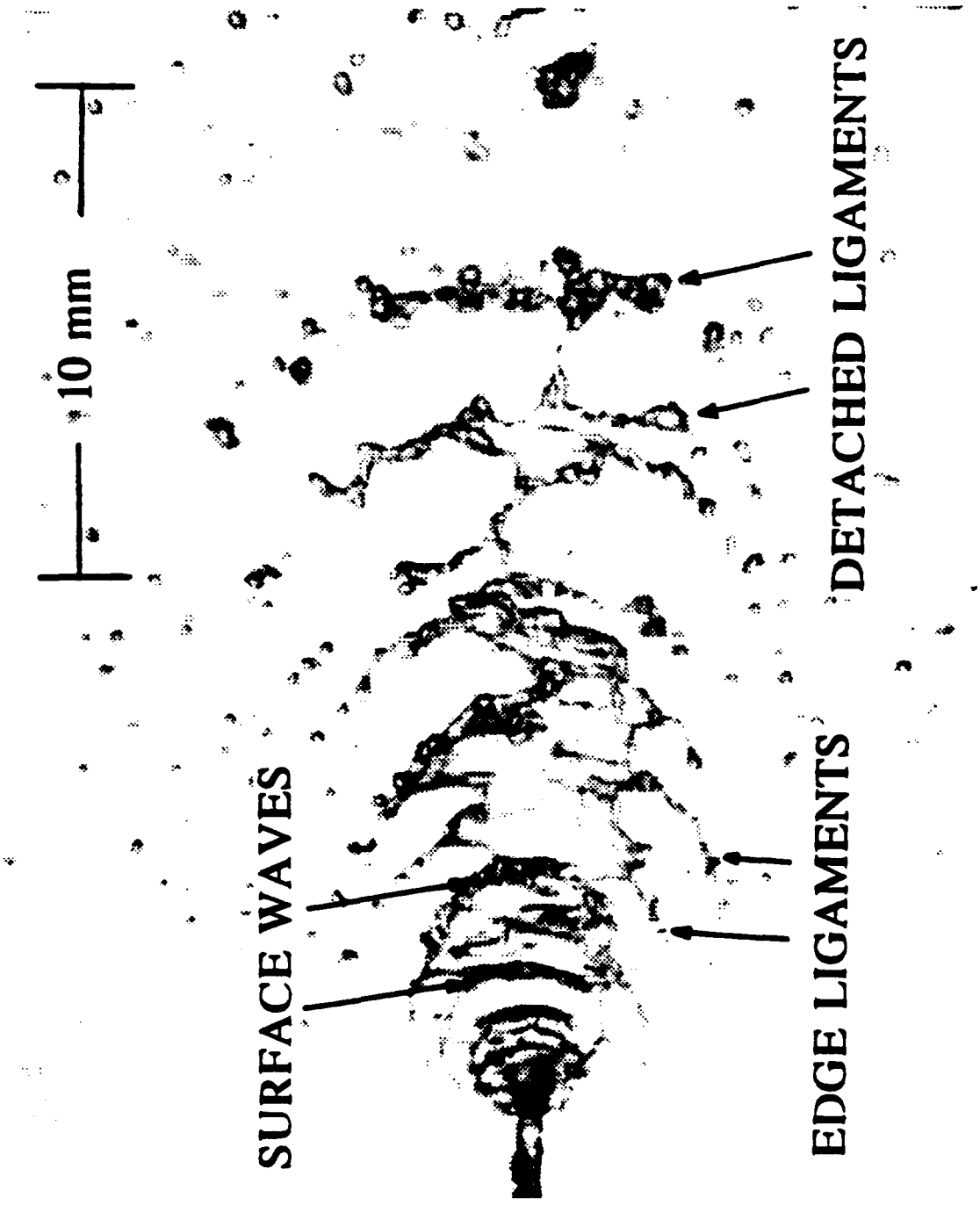

Fig. 9

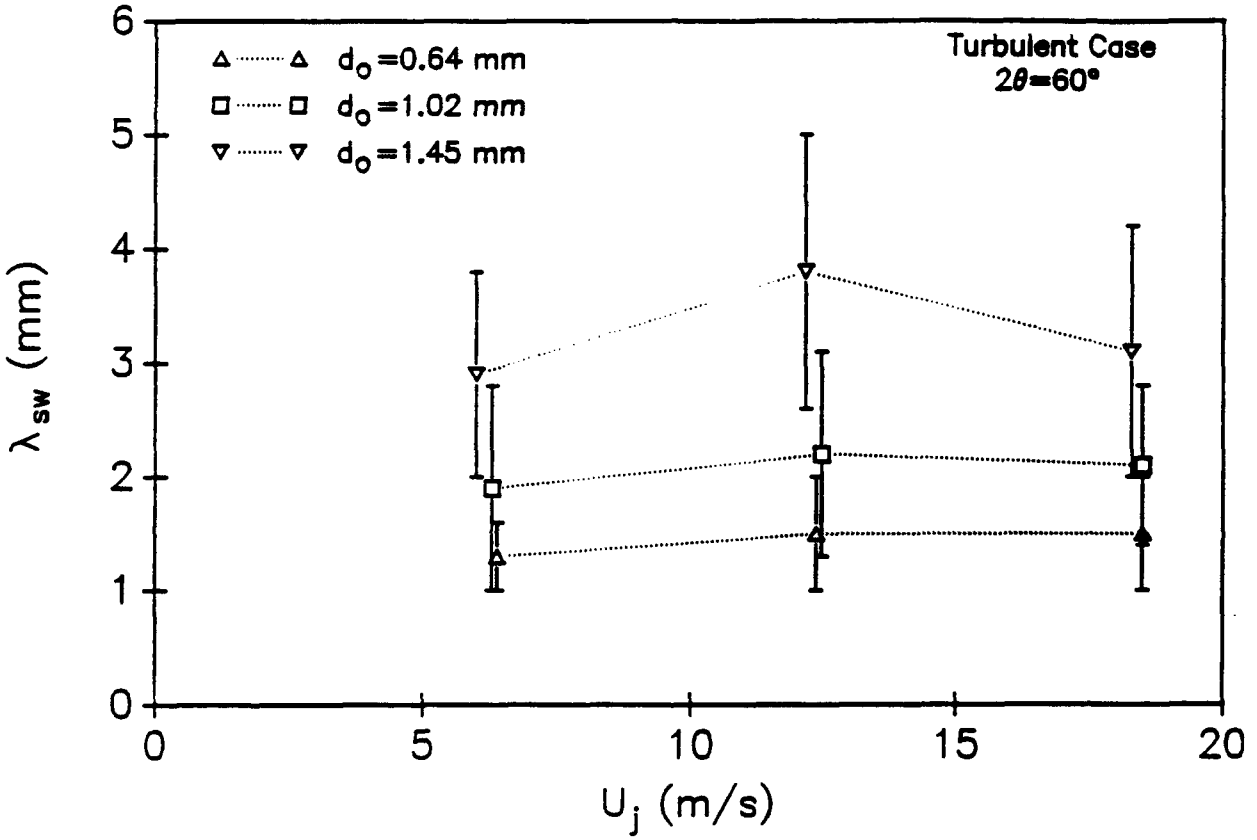
Turbulent Case
2θ=60°
d_o=0.64 mm
d_o=1.02 mm
d_o=1.45 mm
λ_sw (mm)
U_j (m/s)
0
1
2
3
4
5
6
0
5
10
15
20

Fig. 10